Author comments to: The Global Long-term Microwave Vegetation Optical Depth Climate Archive VODCA

Leander Moesinger[1], Wouter Dorigo[1], Richard de Jeu[2], Robin van der Schalie[2], Tracy Scanlon[1], Irene Teubner[1], and Matthias Forkel[1]

[1]Vienna University of Technology, Department of Geodesy and Geoinformation, Gußhausstraße 27-29, 1040 Vienna, Austria
[2]VanderSat, Wilhelminastraat 43A, 2011 VK Haarlem, The Netherlands

Correspondence: Leander Moesinger (Leander.Moesinger@geo.tuwien.ac.at, vodca@geo.tuwien.ac.at)

Formatting as follows:

Reviewers' comments

Reply to comments

[page:line] ~~Deleted parts of the manuscript~~

[page:line] Added/changed parts to the manuscript

1 Response to Xingwang Fan

(1) It is interesting to find that Figure 11 shows an increase of globally-averaged LAI-VOD temporal correlation in the order of C-, X-, and Ku-band. Is this pattern related to the penetration depth of microwave bands, i.e., Ku-band contains more information on top-layer leaves which are captured by LAI? While Figure 6 shows a decrease of globally-averaged LAI-VOD spatial correlation in the same order. Is this pattern related to the relatively homogeneous C-band penetration depth at global scale?

This is very intriguing, we did not realize this before. First thing to note is that for Figure 11 for each location the Spearman correlation between the LAI and VOD time series is calculated and then averaged globally, while for Figure 6 directly the correlation between the hovmoeller diagrams is determined. As such Figure 11 represents the globally averaged temporal correlation, while Figure 6 is related to both spatial AND temporal correlation.
As such we think that the order of correlations in fig 11 is a result of Ku-band and LAI being more affected by the top vegetation canopy than the other bands. However, Figure 6 is a more complicated matter. It could also be that the differences in correlation are due to the differing spatial extent. For example, C-band has more spatial gaps due to more RFI being present than in the other bands. The C- and X-band coverage agrees better with the LAI coverage than Ku-band since all points of a latitude are averaged. Therefore, we should not over-interpret these coefficients. As such we will remove them from the paper to avoid confusion or wrong conclusions.

[12 : 7] ~~The VOD patterns strongly correlate with LAI, quantified by a Spearman coefficient of 0.67, 0.66 and 0.58 between LAI and C-, X- and Ku-band respectively.~~

[14 : 1] ~~the Spearman correlation coefficient is 0.29, 0.29 and 0.26 between LAI and C-, X- and Ku-band anomalies respectively.~~

(2) Instead of jointly retrieving VOD and SSM, is it possible to retrieve VOD using other sources of SSM data, e.g., GLDAS, SMOS and SMAP as inputs? An increase in SSM data quality/consistency likely improves the retrieval of VOD.

Radiative Transfer Model inversion approaches like LPRM aim to retrieve VOD and SSM in a consistent manner that guarantees energy conservation laws. When forcing the retrieval with external soil moisture data sets you also force the VOD to fit the observed brightness temperatures, which is certainly not a guarantee for a good VOD retrieval. LPRM is a proven and tested methodology for retrieving both SSM and VOD simultaneously. For example, using modeled data from a reanalyis data set like GLDAS-Noah or ERA5 would also introduce errors (e.g. related to errors in precipitation forcing) that would directly translate back into the skill of the VOD retrieval. SSM derived from SMAP or SMOS has other uncertainties. In summary, to guarantee consistency and independency of SSM and VOD retrievals, no external SSM data set is used in the retrieval of VOD.

(3) It is a common practice to reduce random errors (noise) by averaging multi-sensor concurrent data. Is it your plan to incorporate more microwave sensors in the future versions of VODCA? Such sensors can include, e.g., FY-3B (X band from 2011-07-12 to present) and FY-3C (X band from 2014-05-29 to present).

We are definitely looking to include as many different sensors as possible to further reduce random errors. But we were not able to get access to Fen Yung data or WindSat data past 2012, even though we would very much like to include it. More realistically, future VODCA versions will include GPM-based retrievals.

(4) Do the anisotropic effects of vegetation absorption/emission play a role in VOD retrieval? That is, to what extent the cosine mapping function (in eq. 2) applies in the 0.25 grid, because this function is derived for horizontally homogeneous canopy. This assumption is generally unsatisfied within the 0.25 grid on the earth surface. Thus, the accuracy of VOD may differ with incidence angle. The MODIS maximum-value compositing NDVI (and then LAI), however, is inclined to select near-nadir pixels. In this sense, the temporal consistency is well maintained. I wonder if LAI-VOD temporal correlation is also affected by land surface heterogeneity which decreases the accuracy of VOD.

Anisotropy primarily plays a role in observations of reflected radiance. This is the case e.g. for solar-reflective observations (bi-directional reflectance distribution function) like those used for MODIS LAI retrievals, or from active microwave observations, which are affected by canopy structure. Emitted radiance can generally be considered anisotrope. For almost all of the currently used soil moisture retrieval algorithms it is an accepted and applied assumption to have polarization-independent VOD. H and V-polarizations do not result in differences in VOD retrievals (Owe et al., 2001) and is actually the basis of LPRM.

The purpose of the maximum-value compositing technique for NDVI data aims to reduce the effects of off-nadir observations and to reduce the effect of low NDVI values on the vegetation signal that are for example caused by snow cover or atmospheric distortions. The maximum NDVI value within a period hence helps to extract a vegetation-sensitive NDVI and to reduce other effects. As VOD retrievals are not affected by snow cover or atmospheric distortions, there is no need to apply the maximum value composite technique to VOD time series (unless there is a biogeophysical interest in maximum VOD values).

2 Response to reviewer #1

2.1 Main discussion points

1) The use of regression-based cdf-matching is argued to be an important component of accurate bias-correcting. This may well be, but as currently written the paper is not convincing. The analysis in Figure 2 is not clear on this front without a label to the color map. Please include a scale bar on this Figure. Even if the numbers are normalized, how much of a difference does it make? 0.5% 1%? 10% 50%? Also, it would be useful to include an additional Figure that shows the exact difference between the: piece-wise CDF-matching and least-squares methods, either by replacing one of the panels or adding it as a third panel. More important, though, is the fact that no comparison between the data set of Liu et al and this new data set is created. In the actual practice of the VOD data set, how closely related are the two data sets? Are there any changes induced to say, the trends? What about other statistics, or simply some sense of say, how often the VOD differs by more than some small threshold (0.05 or so) as a result of this change? Such information needs to be included in several Figures and is crucial not only to judge the improvement created by this new data set, but also towards understanding the quality of the large number of papers that have been written analyzing the Liu et al (2011) data set.

- We did not include a scale bar to the plot because it is a synthetic experiment and as such the absolute values are a function of the parameters (e.g. the distribution the values are sampled from) and therefore not very useful. But we agree that labeling the scale bar would help to get a feeling for the magnitude of the values, see Fig. 1 for new version with a normalized scale bar.

- In response to the comment that it would be useful to include an additional figure that shows the exact difference between the piece-wise CDF-matching and least-squares methods, we tried to make a illustrative figure showing the differences between the two methods. Unfortunately, it ended up being more confusing than helpful. For this reason we suggest to use figure 1 (with the modified scale bar) to show that only the first and last percentile bins are affected.

- Comparing VODCA to Liu et al's data set is a good idea. In the revised manuscript, for several analyses we will compare the finished VODCA products to Liu et al's data set. In summary, we found that the most important difference is that VODCA consists of independent daily observations while the Liu data set seems to have some smoothing applied to the

original observations. This becomes evident for days where no microwave observations are available: In Liu's data set such short-term gaps are filled, although we could not find in literature how this was exactly done.

We see more or less the same trends in VODCA-Ku as in the Liu et al. data set (Fig. 2). Using daily data, the Liu data set correlates more strongly with LAI than VODCA (Fig. 3, left column), probably because of the applied temporal smoothing. But if both data sets are downsampled to monthly time steps, VODCA correlates more strongly with LAI than Liu et al's data set (Fig. 3, right column). Based on our analyses we conclude that papers written on the basis of Liu et al's data set are still valid, but that VODCA will add value to future studies because it covers a longer time span, has temporally-independent daily VOD values, provides separate products for different frequencies, and reduced noise.

We will include the comparison of the VODCA data set with Liu's data. The main changes to the manuscript will be:

- Page 17, subsection "4.4.1 Correlation between VOD and LAI" now also compares Liu et al's data set with LAI.
- Updated most hovmoeller (see fig. 4) plots to also include Liu et al's data set. We will not update the fractional coverage hovmoeller, as the smoothing present in Liu et als data set leads to inflated values.
- Added figure 2 to section "4.4.2 Trend—analysis of VOD, LAI and Vegetation Continuous Fields" with description.

2) Figure 7 on page 14: The values mentioned in the text here are pretty low Spearman correlations so it is difficult to test if the LAI anomalies line up with the VOD anomalies or not. Furthermore, this analysis in and of itself does not indicate successful bias removal. It would be more useful to focus instead on whether there are any changes at the breakpoints in when different data sets are available (which are known a priori) rather than comparing across the entire record. Please use the methods developed for soil moisture in Su et al, Geophysical Research Letters, 2016 ("Homogeneity of a global multi-satellite soil moisture climate data record") to test for breakpoints.

We agree with the reviewer that computing the correlations per "blending period" gives more insight in the skill to detect anomalies per period. Due to the absence of a VOD reference data set, the Su et al methods cannot be applied. Instead, we calculated the correlation of VODCA and LAI for the different blending period, similar to Dorigo et al. (2015). The results (Fig. 5) show that the spatial distribution of the correlation between VOD and LAI is time-invariant for all VODCA bands. This demonstrates that the temporal dynamics are consistent over the whole time period.

Correlation analysis between LAI and VOD per blending period (fig. 5) will be added to the results.

3) I strongly urge the authors to reconsider the choice not to include daytime retrievals in the VODCA (page 4, line 20). While the idea that daytime retrievals are more error-prone because of greater differences between soil and canopy temperature is common in the microwave radiometry community, few studies have been done document the extent of this error. Recent results suggest, for example, that PM soil moisture retrievals are not always more error-prone than AM ones (particularly under densely vegetated conditions), see Fan et al, Remote Sensing, 2015 ("The Impact of Local Acquisition Time on the Accuracy

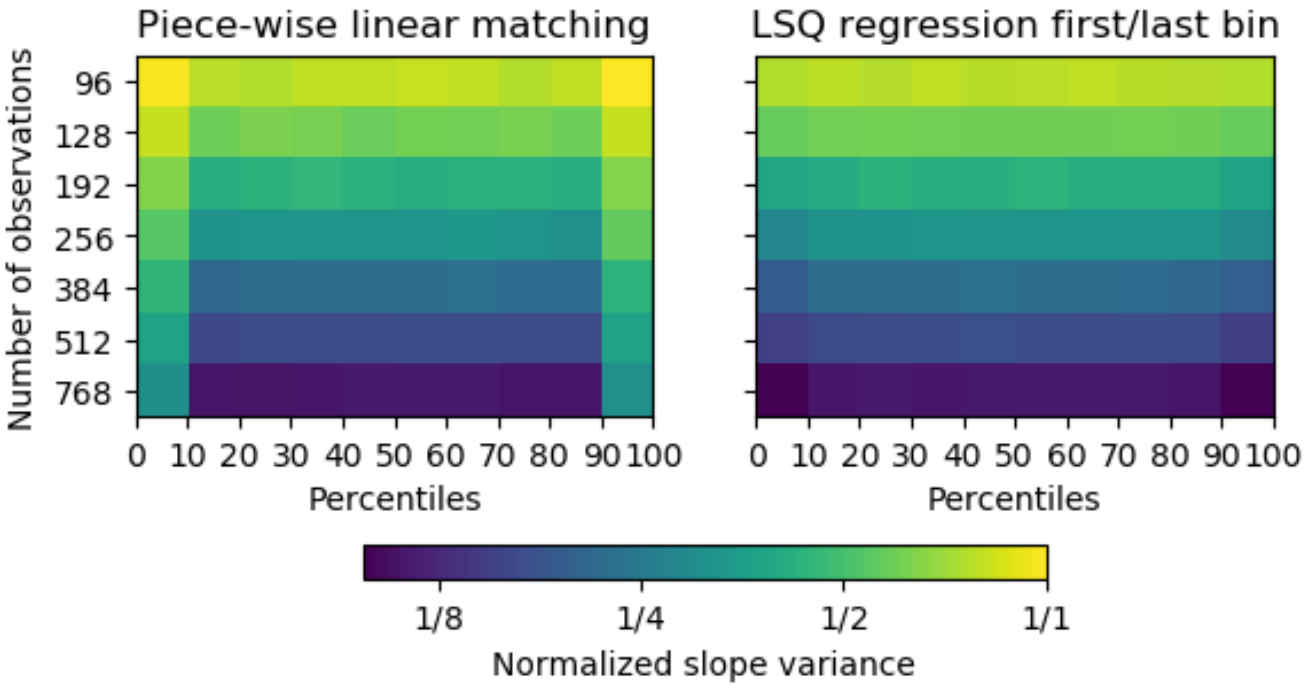

Figure 1. Reworked figure 2: Simulated variance of slopes of old a new CDF matching method. New are the scale bar tick labels

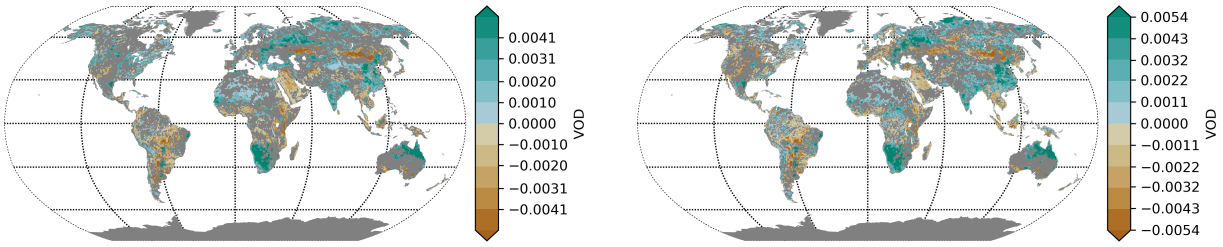

(a) Liu et al trends

(b) VODCA-Ku trends

Figure 2. Liu et al and VODCA trends from 1993-01 to 2012-12 (will be included in revised manuscript).

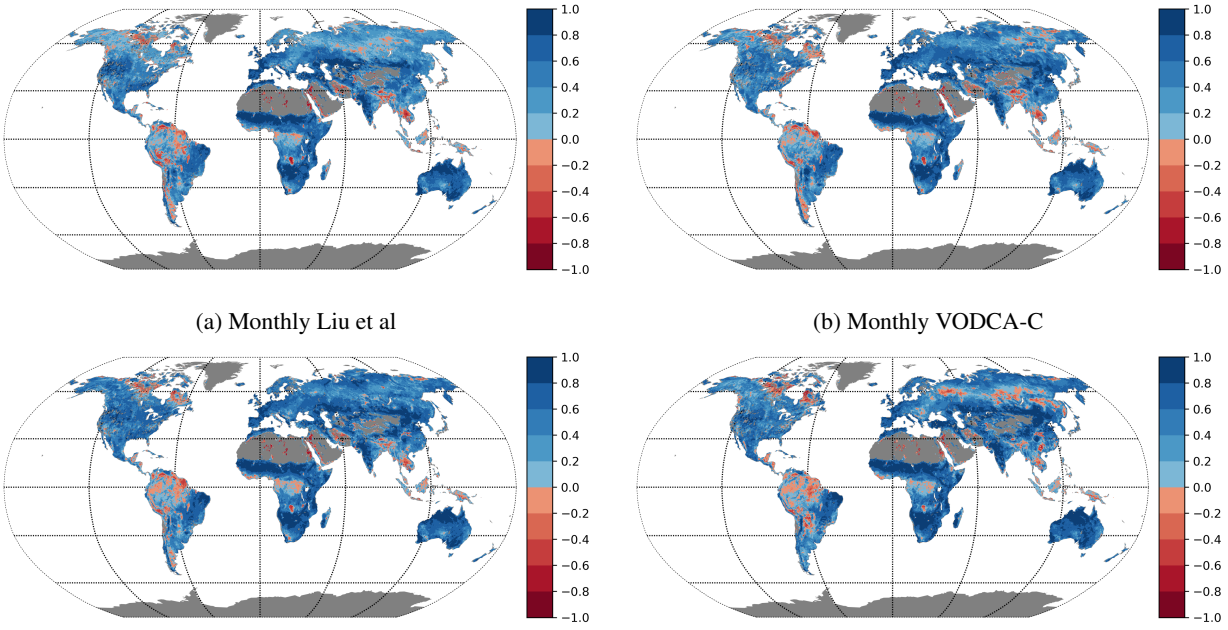

(a) Monthly Liu et al

(b) Monthly VODCA-C

(c) Monthly VODCA-X

(d) Monthly VODCA-Ku

Figure 3. Correlation of monthly LiuVOD and the VODCA products with MODIS LAI. For this analysis, the data are first resampled to monthly averages, then only the months where all four data sets have values are used.

of Microwave Surface Soil Moisture Retrievals over the Contiguous United States"). Given the significant potential for diurnal changes in VOD to be useful for studying vegetation water stress (see Konings and Gentine, Global Change Biology, 2017 ("Global variations in ecosystem-scale isohydricity"), such a data set could be quite useful. A flag could still be included for the nighttime data to suggest greater uncertainty.

While technically it would be possible to produce a daytime product using the same methods, the daytime LPRM-VOD products are still very experimental. Currently, we don't want to release a daytime product to prevent users from making false scientific conclusions based on potential data artifacts. Our experience from ESA CCI Soil Moisture has taught us, that despite providing quality flags and extensive documentation, many users do make wrong use of data sets. A release of daytime products requires a proper evaluation, a comparison with nighttime products and an assessment of differences. Such an analysis is beyond the scope of this paper. However, we consider such an analysis essential and will likely address it in the near future. Once our scientific understanding and confidence in the day-time products is mature enough, we will include this in a future release of VODCA.

4) Relatedly (page 7, line 14), the above-cited Konings and Gentine paper has shown there is a significant expected diurnal cycle in VOD (see also Konings et al, Geophysical Research Letters, 2017 "Active microwave observations of diurnal and

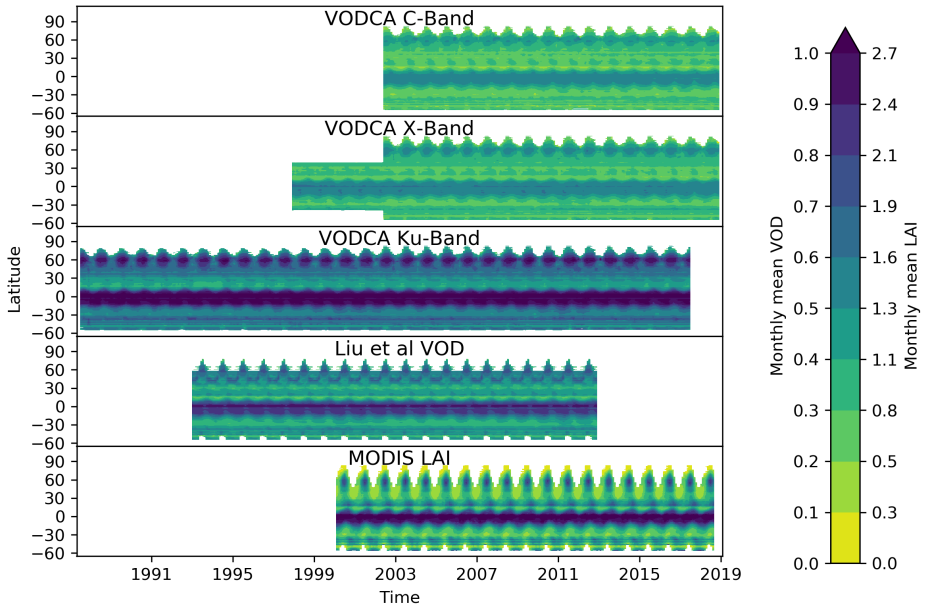

(a) Mean

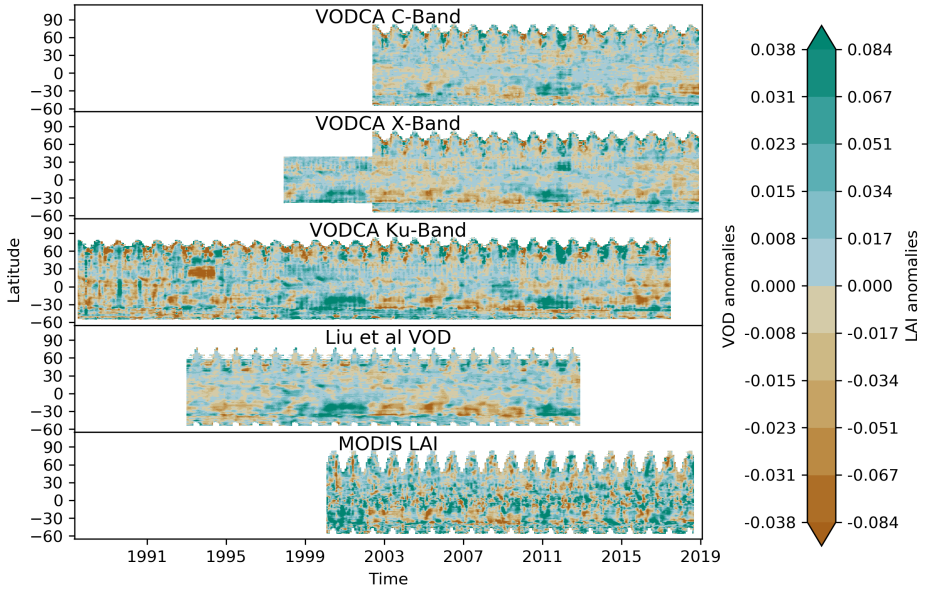

(b) Anomalies

Figure 4. Hovmoellers diagrams of monthly VOD values (top) and monthly VOD anomalies (bottom) including the merged VOD dataset by Liu et al.

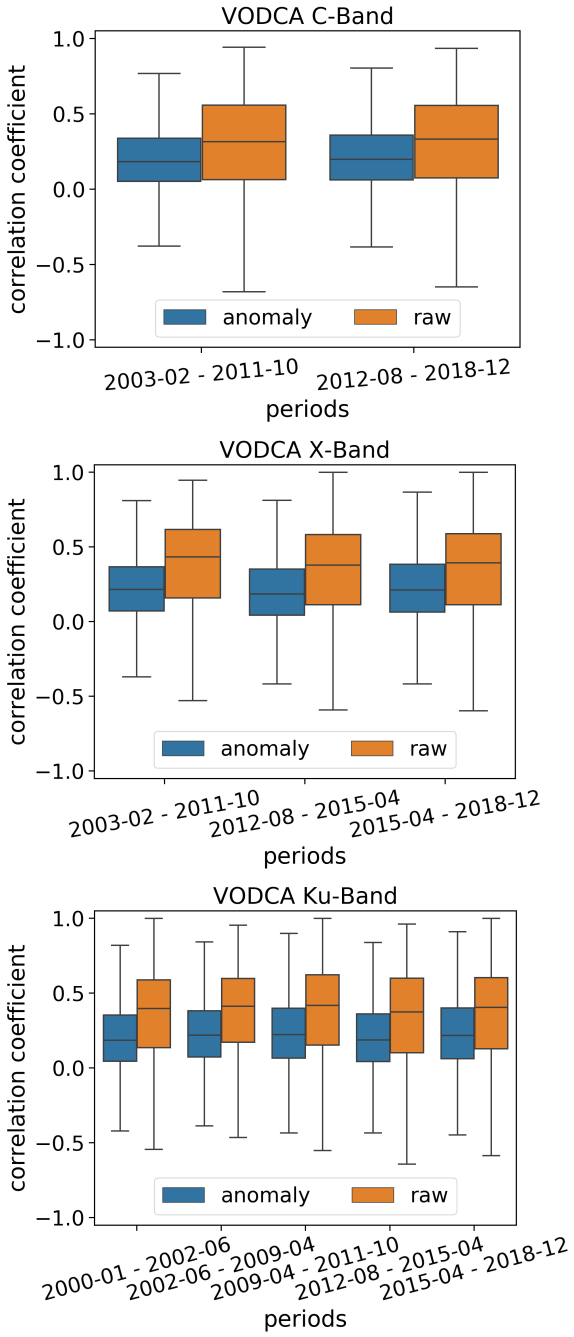

Figure 5. Correlation between VODCA and MODIS LAI, raw time series and anomalies, for different blending periods.

seasonal variations of canopy water content across the humid African tropical forests" for the active equivalent of this, with more complete diurnal measurements). As such, presenting the data to be "resampled to a specific time" as in page 7, line 14, is misleading. At the very least, the data should be presented as averaged over a certain period. If that is the case, and if the authors really insist on not using daytime data, it would still be cleaner to just present it as a day-long average.

We concur, this is a bit poorly worded and can be misunderstood.
We are adjusting the relevant passages of the manuscript to talk of "nightly averages" instead.

5) Little literature exists on whether sensor differences are really more significant than algorithmic differences. This may explain why SMOS and SMAP baseline retrievals were found by the authors to have little consistency; those retrieval algorithms are fairly different – not something specific about L-band frequency. L-band VOD has been shown to have significant utility over X-band and likely C-band (see Brandt et al, Na-ture Ecology and Evolution, 2018 "Satellite passive microwaves reveal recent climate-induced carbon losses in African drylands"). While I recognize that it may genuinely be impossible to create an L-band product using the methodology employed here (without re-running the LPRM on SMOS and SMAP so that a common algorithm is present), a more detailed treatment should be provided than just lines 21-23 on page 3. Please make it clear that it is not possible for you to create the L-band product, not "does not warrant a product for it", which suggests L-band data is not useful. Also, can you include the low temporal correlation in a supplemental plot?

We agree that a more sophisticated argumentation would be appropriate at this point. Also Reviewer #2 was pointing this out. In a preliminary analysis, we used L-band VOD products from SMAP and SMOS retrieved with LPRM. The temporal correlation between the daily LPRM-SMOS and LPRM-SMAP values is very low (globally in average about 0.1, while the correlation coefficients in the other bands achieved values of 0.6 to 0.7, Fig. 6). Lower temporal dynamics and hence correlations are expected for L-band in comparison to shorter wavelengths because L-band largely penetrates the canopy with strong seasonal changes in leaf biomass and is more sensitive to the woody parts. Hence, the relatively small intra-annual dynamics are more sensitive to noise in the data. This is not a problem exclusive to LPRM-derived L-band VOD products. To the best of our knowledge, all studies involving L-band VOD use temporally averaged data rather than using daily values. For example, Brandt et al. (2018) averaged all SMOS-IC data between 2010 and 2016 and analyzed only spatial correlations, disregarding temporal dynamics.
We also applied the VODCA merging procedure to L-band VOD data from LPRM-SMAP and LPRM-SMOS. The autocorrelation analysis showed that the obtained VODCA-L-band VOD has a lower temporal autocorrelation than the original LPRM-SMAP VOD (Fig. 7). This indicates that the level of noise in L-band was increased with the merging. Hence for L-band, the merging results in a lower-quality data set. In addition, the low density of observations in LPRM-SMOS causes a highly unbalanced temporal coverage of VOD values (Fig. 8). Given this unbalanced data coverage there is a high risk that users might wrongly use this dataset for e.g. trend analysis. However, we are convinced that there is a large potential to produce a more reliable multi-sensor/multi-product merged L-band data set in the future, e.g. by using alternative L-band retrievals

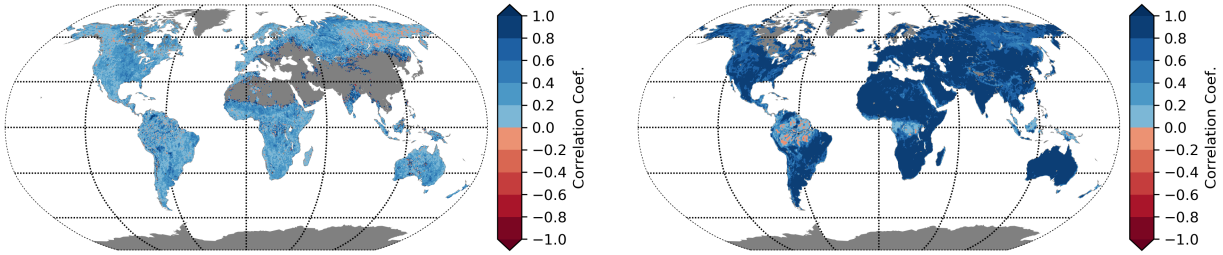

(a) L-band LPRM-SMAP vs. LPRM-SMOS

(b) Ku-band AMSR-E vs. WindSat

Figure 6. Correlations between different sensors of the same band. The Ku-band WindSat vs. AMSR-E plot is similar to all other sensor combinations in the Ku, X, and C band.

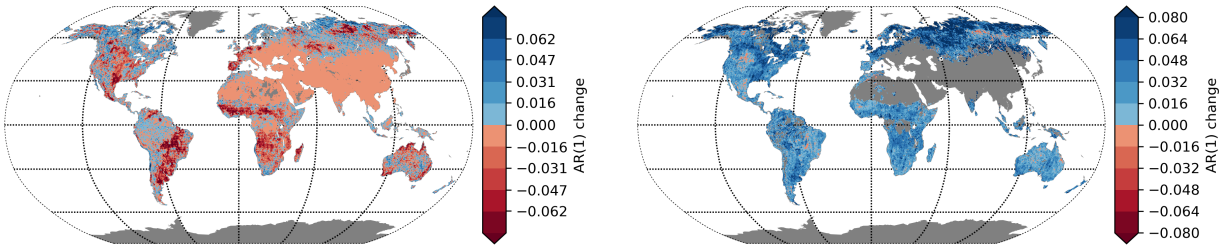

(a) SMOS change

(b) SMAP change

Figure 7. Ar(1) change of SMAP and SMOS due to merging. Note that the original SMAP time series has less noise than experimental VODCA-L

from SMOS-IC or MTDCA. Yet, the current VODCA methodology cannot be easily applied to L-band data. Hence alternative blending approaches first need to be thoroughly assessed, which goes beyond the scope of the current paper.

We will add a paragraph in the introduction explaining in detail the reasoning behind not producing VODCA-L. We will also include figures 6 and 7 in the supplement for that purpose and expand the discussion regarding the possibility of an L-band product. We will also take care to talk specifically of LPRM-L-VOD and not L-VOD in general.

2.2 Minor discussion points

1) Section 3.1 Regarding the 2 AMSR2 C-band channels: was any statistical evaluation done to see how different the retrievals from the two channels were, when taken in isolation?

VOD from the two C-band channels from AMSR2 is highly correlated (Fig. 9), so using 7.3 GHz instead of 6.9 Ghz will have little impact. Actually, the 7.3 GHz channel was purposely added to AMSR2 to mitigate RFI in the 6.9 GHz channel. We

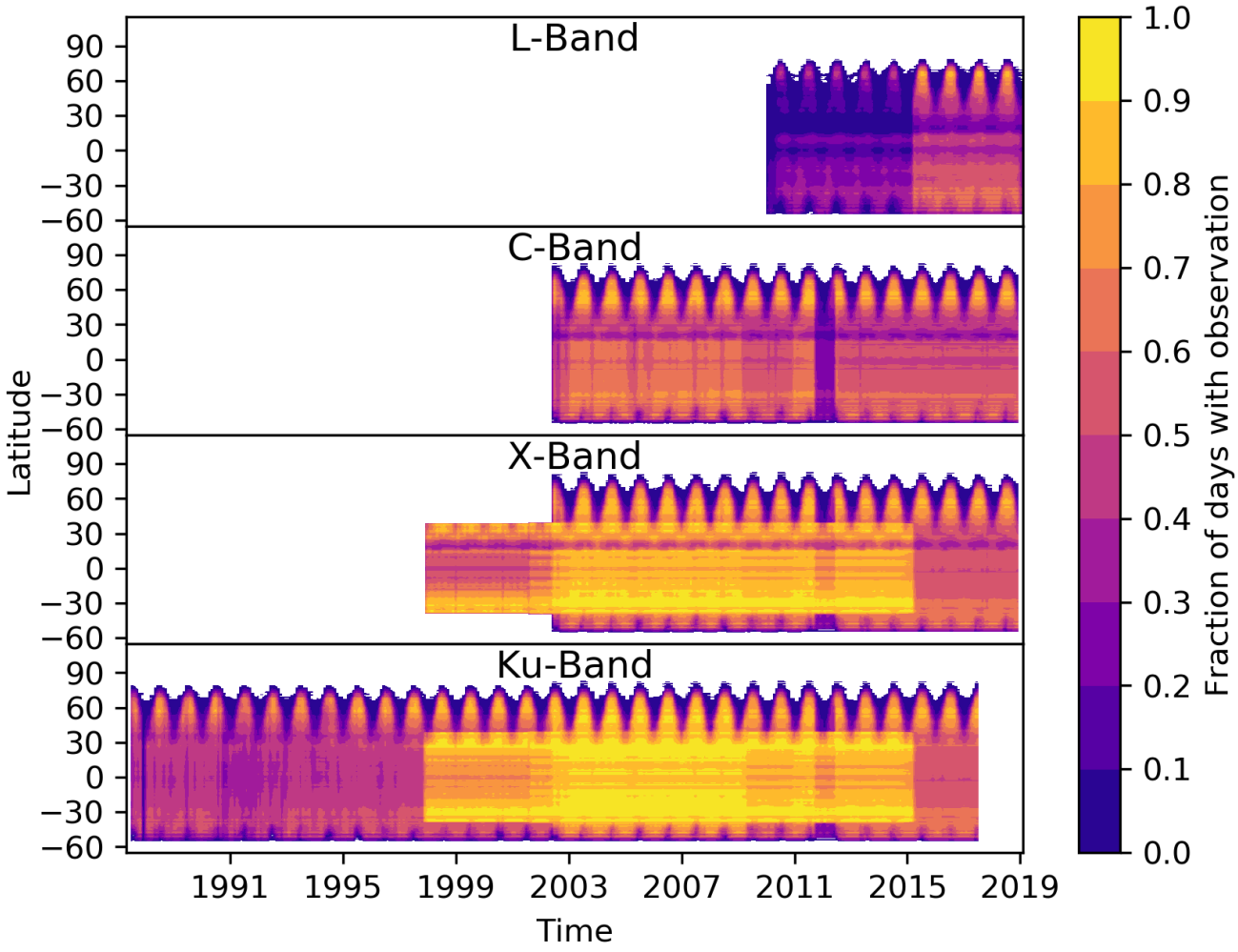

Figure 8. Fractional coverage hovmoeller plot, also including experimental VODCA-L.

will add this plot to the supplement and add to the main text:

[8 : 3] As the two C-bands are highly correlated, the use of one or the other has a minor impact on the quality of the dataset (Fig. 9).

2) Page 9 lines 2-3: Please provide more information on how the bin sizes are chosen.

Agreed, this is in need of some clarification. We added following sentences to the end of the relevant paragraph:

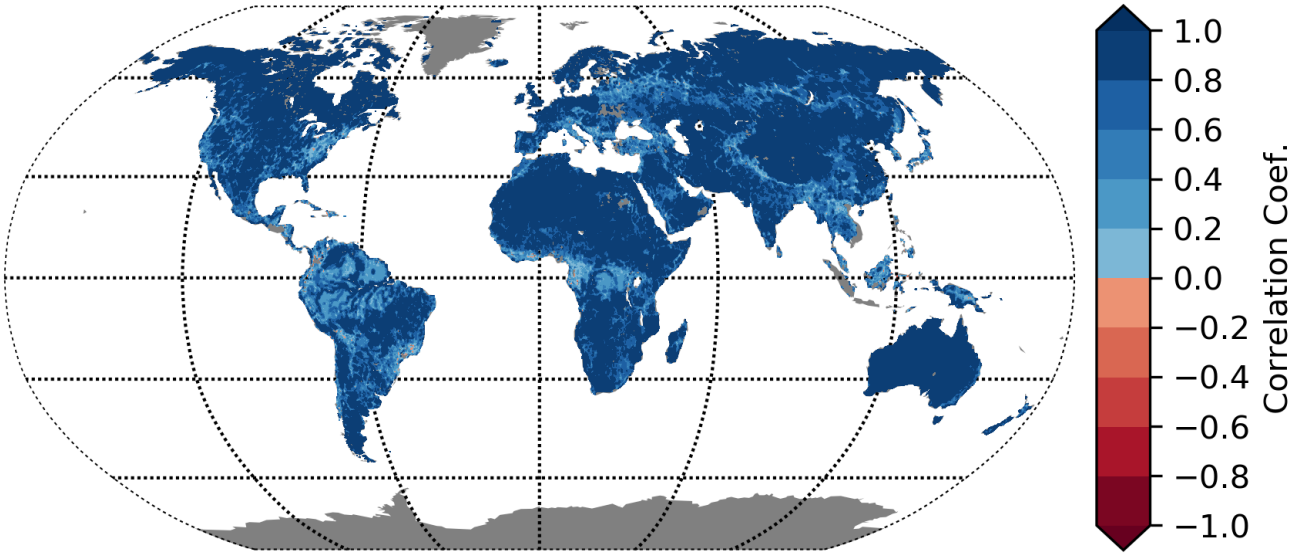

Figure 9. Correlation between the AMSR2 6.9 and 7.3 GHZ band

[9 : 2] The bin size of 20 was chosen as compromise between data coverage and often used bin sizes. A bin size of 50 observations is often used as a rule of thumb for univariate regression to get robust estimates (Green, 1991). However, our main goal was rather to prevent time series with very few observations from learning spurious scaling parameters and we also did not want to loose all time series with less than 50 values. As such 20 was chosen as a compromise.

3) Page 10 line 11: How often does removal of such unphysical values happen? This is important information as these values are made unphysical as a direct consequence of the cdf-matching variant employed here.

A fraction in the order of $1/10^6$ to $1/10^8$ of values are lost this way, so almost nothing gets lost. Anyway, the only way to prevent any CDF-matching technique to produce values below zero is to force its intercept trough zero. But this would mean that potentially it becomes a very bad fit for the value range where the data is actually located. We added the clarification to the manuscript.

[10 : 11] These values are deemed unreliable and are removed. However, this occurs very rarely, only a fraction of about $1/10^6$ to $1/10^8$ of values are lost in this way.

4) Page 10, line 1-2: How many observations is deemed enough? Please include in text (not just Figure 3 for clarity. Relatedly, Figure 3 is not consistent with the text in Section 3.2.4 (since for example, the figure pseudo-code does not mention the

use of the first and last two years). This makes it actively confusing – please make sure Figure 3 is fully complete.

As a threshold, we used the same number of observations as for the bins reported on Page 9 lines 2-3, i.e. 20 (otherwise the matching may become too unreliable).

About Fig. 3: The usage of the first/last 2 years is mentioned in the pseudo-code but we agree that it does not mention that the minimum of 20 observations need to come from the last two years of AMSR-E and the first two years of AMSR2. But anyway, since reviewer M. Piles finds the Figure unnecessary and we also were never content with it, we will remove Figure 3 entirely without replacement.

Figure 3 will be removed from the manuscript.

3 Response to Maria Piles

3.1 Main discussion points

1. Their approach for the merging builds from the one used for the ESA CCI Soil Moisture product and the previous long-term VOD product from Liu et al., 2011, with improvements to make it more robust to the presence of outliers. The improvement shown with respect to the previous version is not convincing. What is the numerical range of the colorbar in Fig. 2? Can the authors also show results with real data? Also, the authors say (page 8, line 31) they dynamically increase the step size of the percentiles "if only a few" observations are available. It would be important to be more specific here and show how the method is sensitive to the choice of this parameter. In general, an improved characterization of their matching approach is needed.

We agree that Figure 2 does not give a full insight into the improvements of the methods. However, with the lack of any reference data, making some test with real data is unfeasible. Using synthetic data has the advantage that the results are not skewed by some external effect, but only depend on the methods used. These simulations show that for exactly the same set of input data, the new CDF-matching method gives much more reliable scaling parameters for the first and last bins. We will add a normalized scale bar for reference to quantify the change. A bin size of 20 was chosen as compromise between data coverage and often used bin sizes. A bin size of 50 observations is often used as a rule of thumb for uni-variate regression to get robust estimates (Green, 1991). However, our main goal was rather to prevent time series with very few observations from learning spurious scaling parameters and we also did not want to loose all time series with less than 50 values. As such 20 was chosen as a compromise.

[9 : 2] The bin size of 20 was chosen as compromise between data coverage and often used bin sizes. A bin size of 50 observations is often used as a rule of thumb for uni-variate regression to get robust estimates (Green, 1991). However, our

main goal was rather to prevent time series with very few observations from learning spurious scaling parameters and we also did not want to loose all time series with less than 50 values. As such 20 was chosen as a compromise.

2. The authors report there is a flag indicating the matching method (page 10, line 8) and a flag indicating which sensors contributed to a measurement (page 11, line 2). It would be very useful if they could relate those flags to the quality of the final product and make recommendations to the user. Perhaps the authors could consider dedicating a specific section of the paper to their quality flags and assessment.

First of all, we want to point out that right now only the C-band can have any bad quality flags due to irregular processing, the other bands always use the standard processing chain. The 6.9 and 7.3 GHz C-bands are highly correlated (Fig. 9), showing that using the lower frequency instead of 6.9 GHz has little impact on the results. For the other flags it is really hard to make any recommendations as they depend a lot on what the data are used for and there is a wide range of possible uses that we cannot foresee. Still, we will add to the supplement a summary of all available quality flags.

Supplement: We added a section about quality flags, their meaning with links to relevant sections in main text.
In main text, following line is added together with the figure:

[8 : 3] As the two C-bands are highly correlated, the use of one or the other has a minor impact on the quality of the dataset (Fig. 9).

3. I would strongly recommend the authors to consider including the daytime observations to the data set. Although it is well-known that daytime retrievals are expected to have a higher error than nighttime ones due to the thermal equilibrium assumed in the inversion, the difference between day and night canopy water have been shown useful for certain science studies (e.g. see Konings & Gentine, Global variations in ecosystemscale isohydricity, Global Change Biology, 2016). Also, their combination could be potentially useful for some applications to enhance the temporal coverage.

While technically it would be possible to produce a daytime product using the same methods, the daytime LPRM-VOD products are still very experimental. Currently, we do not want to release a daytime product to prevent users from making false scientific conclusions based on potential data artifacts. Our experience from ESA CCI Soil Moisture has taught us, that despite providing quality flags and extensive documentation, many users do make wrong use of data sets. A release of daytime products requires a proper evaluation, a comparison with nighttime products and an assessment of differences. Such an analysis is beyond the scope of this paper. However, we consider such an analysis essential and will likely address it in the near future. Once our scientific understanding and confidence in the day-time products is mature enough, we will include this in a future release of VODCA.

4. The validation does not show the value of the multi-frequency retrievals, nor discusses in detail their differences with respect to the optical indicators they selected. The authors should elaborate more on their results with focus on the different bands and perhaps consider a comparison of the sensitivity of the different VOD to biomass (e.g. see Nemesio-Rodríguez et al., biogeosciences, 2018)

While we are eager to analyze the usability of the different frequencies for various applications, this is not the focus of a data set paper. The primary goal of the manuscript is to introduce the new VODCA data set, give insights into its methodology, and demonstrate in various ways if the values we produce and the dynamics that we see in the data set are plausible. This focus is also outlined in the aims and scope of the journal: https://www.earth-system-science-data.net/about/aims_and_scope.html. Focusing too much on the interpretation of the results would derail the topic and further increase the length of the paper (it already now is on the long side).

3.2 Minor discussion points

1. Page 1, line 10. The authors should introduce in the abstract the previous long-term VOD data set and clarify the novelties of their newly presented data set, i.e. frequency-specific VOD, extended period, improved matching.

While Liu et al's data set has a much more prominent role in the revised manuscript, the abstract becomes too long and confusing if we describe two VOD data sets and their differences already there. However, the extended period, the new matching technique, and the separate frequency-specific VOD data sets are already mentioned.

2. Page 1, line 24. Is the trend measured by all frequencies? Are there any differences? It would be nice to complement the validation and include the value of having frequency-specific VOD here.

Thanks for the suggestion, this is indeed something that needs to be specified. We only looked at Ku-band long term trends (because it is 10 years longer than X-band).

[1 : 24] We added: "Trend analysis of Ku-Band VODCA shows that between 1987 and 2017 there has been ..."

3. Page 2, line 2. The authors could (at least) indicate how the multi-frequency VOD could actually complement optical measurements (e.g. canopy water vs. greenness)

This is a good idea, we added a sentence on the uniqueness of the observations.

[3 : 2] We added: "In summary, VODCA shows vast potential for monitoring spatial-temporal ecosystem changes complementary to existing long-term vegetation products from optical remote sensing as VOD is unaffected by cloud cover or high sun zenith angles. In addition, VOD is sensitive to vegetation water content and hence complements optical indices of vegetation greenness and leaf area.

4. Page 2, line 14. Additional references are needed in the intro and the discussion regarding multi-frequency VOD estimates and sensitivity to different parts of the canopy. I point out two articles hereafter, but recommend nonetheless the authors to do a bibliography search: F. Tian et al., Coupling of ecosystem-scale plant water storage and leaf phenology observed by satellite, nature ecology and evolution, 2018N. Rodríguez-Fernández et al., An evaluation of SMOS L-band vegetation optical depth (L-VOD) data sets: high sensitivity of L-VOD to above-ground biomass in Africa, biogeosciences, 2018

Thanks for the suggestion, we added your proposed as well as additional references.

Changed sentence: Short wavelengths experience a higher attenuation by vegetation (and hence relate to higher VOD values) than longer ones (Liu et al., 2009; Owe et al., 2008; Kerr et al., 2018). As a consequence, VOD estimates from long wavelengths are sensitive to deeper vegetation layers (e.g. stem biomass) while VOD estimates from short wavelengths are more sensitive to canopy moisture content (Chaparro et al., 2018; Tian et al., 2018; Fan et al., 2018; Konings et al., 2019).

5. Page 3, line 23. Do the authors mean there is a low temporal correlation of SMAP and SMOS VOD products? Which products? Please, provide appropriate references or supporting material for this statement. Perhaps the addition of L-band could be directly included as future work, latest products from the two missions (SMAP MTDCA and SMOS-IC for instance) seem to agree well.

We agree that a more sophisticated argumentation would be appropriate at this point. Also Reviewer #1 was pointing this out. In a preliminary analysis, we used L-band VOD products from SMAP and SMOS retrieved with LPRM. The temporal correlation between the daily LPRM-SMOS and LPRM-SMAP values is very low (globally in average about 0.1, while the correlation coefficients in the other bands achieved values of 0.6 to 0.7, Fig. 6). Lower temporal dynamics and hence correlations are expected for L-band in comparison to shorter wavelengths because L-band largely penetrates the canopy with strong seasonal changes in leaf biomass and is more sensitive to the woody parts. Hence, the relatively small intra-annual dynamics are more sensitive to noise in the data. This is not a problem exclusive to LPRM-derived L-band VOD products. To the best of our knowledge, all studies involving L-band VOD use temporally averaged data rather than using daily values. For example, Brandt et al. (2018) averaged all SMOS-IC data between 2010 and 2016 and analyzed only spatial correlations, disregarding temporal dynamics.
We also applied the VODCA merging procedure to L-band VOD data from LPRM-SMAP and LPRM-SMOS. The autocorrelation analysis showed that the obtained VODCA-L-band VOD has a lower temporal autocorrelation than the original

LPRM-SMAP VOD (Fig. 7). This indicates that the level of noise in L-band was increased with the merging. Hence for L-band, the merging results in a lower-quality data set. In addition, the low density of observations in LPRM-SMOS causes a highly unbalanced temporal coverage of VOD values (Fig. 8). Given this unbalanced data coverage there is a high risk that users might wrongly use this dataset for e.g. trend analysis. However, we are convinced that there is a large potential to produce a more reliable multi-sensor merged L-band data set in the future, e.g. by using alternative L-band retrievals from SMOS-IC or MTDCA. Yet, the current VODCA methodology cannot be easily applied to L-band data. Hence alternative blending approaches first need to be thoroughly assessed, which goes beyond the scope of the current paper.

We added a paragraph in the discussion explaining the reasoning behind not producing VODCA-L. We also included figures 6 and 7 in the supplement for that purpose and expand the discussion regarding the possibility of an L-band product. We will also take care to talk specifically of LPRM-L-VOD and not L-VOD in general.

6. Page 4, line 10. A reference to the tau-omega model is needed. Please include: T. Mo, B. Choudhury, T. Schmugge, and T. Jackson, “A model for microwave emission from vegetation-covered fields,” J. Hydrol., vol. 184, no. C13, pp. 101–129, Dec. 1982

We already referenced this paper just before at line 5 but we agree that it is not prominently enough. We changed the sentence:

"LPRM v6 (van der Schalie et al., 2017; Owe et al., 2008; Meesters et al., 2005) retrieves soil moisture and VOD at the same time from vertical and horizontal polarized microwave data and is based on a radiative transfer model first proposed by Mo et al. (1982).
The model assumes..."

7. Table 1: It would be interesting to add ascending and descending times for each sensor as well as their incidence angles, spatial and temporal resolutions. The authors could perhaps add a little discussion on the impacts of mixing the different times and observation geometries (spatial resolution, incidence angle, etc).

This is a very good idea, we added the equatorial crossing times to the table - for more there is unfortunately not enough space. Unfortunately not much knowledge is currently available regarding the effect of mixing VOD observations, therefore we added a paragraph to the discussion.

- Updated table with equatorial crossing times
- Expanded discussion with a subsection (5.5) about VOD merging.

8. Page 4, line 24: it is unclear how the different data sets can be accessed (web-page?). Please, specify which ones are available and which ones are not (perhaps on Table 2 also).

Agreed, this is necessary information in a data set paper.

We added following paragraph:

[4 : 24] While LPRM v6 is not publicly available, older versions are available trough GFSC: https://disc.gsfc.nasa.gov/datasets/LPRM_AMSR2_D_SOILM3_001/summary

9. Page 9, Line 25. I understand AMSR-E is used as a reference for having the highest overlap. But perhaps AMSR-2 could also be chosen for being a more advanced instrument with improved capabilities, or also a modeled VOD could potentially be used. Please, include a discussion for this choice (or provide a reference) and why it was chosen over the alternatives.

AMSR2 has a very similar design and skills as AMSR-E but has only little overlap with the other data sets. We do not want to use modeled VOD as a reference as we want to stay as close to the observations as possible. Using modeled VOD may introduce biases, e.g. related to uncertainties in the forcing data set.

We added a reference to CCI SM which uses AMSR-E as reference for the same reason.

10. Page 6, line 1. Please, indicate how to access the ancillary data used in the corresponding subsection (LAI and VCF).
We added the links to it (they already were in the acknowledgements and references).

11. Page 6, line 4. What do the authors expect from the comparison of VOD and LAI? A rationale of why they chose LAI over other indices (e.g. NDVI, EVI) and whether they expect a higher correlation with any of the specific VOD products is needed

It serves two purposes. Mainly, the lack of ground truth makes the validation of VOD data difficult. At field studies with different crop types, it has been shown that VOD is closely related to LAI (Sawada et al., 2016). LAI has been also used to assess other VOD products from active sensors (Vreugdenhil et al., 2017). For the assessment of VOD, we prefer LAI in comparison to NDVI because NDVI saturates earlier at high biomass levels than LAI. However, we do not expect the correlation to be very high as, as you mentioned earlier, LAI is a measure of leaf area while VOD is related to vegetation water content. As the higher frequencies (Ku-band) are more sensitive to the vegetation canopy than the low frequencies (L-band), we expect higher correlations between Ku- and X-band VOD with LAI than between L-band VOD and LAI.

We expanded the motivation a bit to explain better why LAI was chosen.

12. Page 7, line 8: How is the VOD climatology from AMSR-E derived? Please provide details.

This paragraph is just a summary, the details are in the subsequent subsection. By climatology we mean that if a sensor observes a specific combination of earth surface properties, LPRM will derive a specific VOD value. However the use of the term climatology is truly confusing in this context.

Alternatively we propose:

[7 : 8] Second, bias between the different sensors is corrected for by scaling them to VOD from AMSR-E C-, X-, and Ku-band, respectively.

13. Page 7, line 26. I agree with the authors that negative VOD retrievals are physically impossible. However, they are most probably linked to uncertainties/simplifications on the physical model used in the inversion, and their direct truncation may lead to erroneous trends for specific areas. One alternative could be to let the user truncate the values after temporally averaging the data set according to the needs of their study. This is the procedure followed for instance in the SMOS-IC product (Fernández-Moranet al., remote sensing, 2017). I would ask the authors to consider this option or at least, mention it in the discussion.

We agree that your proposed method is the correct way to release a data set based on a single sensor, and we also thought about doing it this way. But the trouble is that we average multiple sensors and redistribute only the averaged values. If we average the negative values with positive values from other sensors, we are averaging two observations with very little confidence in one of those. This leads to a lower-quality average than if we just discarded the negative value. We also considered to keep negative values if no other sensor has a valid value at that date. But that would mean that the time series will be spliced with values that are both negative AND are the result of only one sensor and therefore are of a lot lower quality than the other values in the time series. We might do something like that in a future version, but there are many open questions to it; it would also require a large rework of the code.

14. Page 8, line 2. How different are the retrievals from the two C-band channels? Again the authors include a flag but this flag is not useful if it is not related to a quality indicator or any further recommendation is given.

We agree and calculated the temporal correlation between the C1 and C2 band, which are strongly correlated (Fig. 9)

Addition to manuscript (inclusive figure which isin supplement):

[8 : 3] As the two C-bands are highly correlated, the use of one or the other has a minor impact on the quality of the dataset (Fig. 9).

15. Page 8, line 22. I infer from the text that there is a need to a new cdf-matching technique due to the presence of outliers in the VOD data set. Could this cdf-matching also improve the VOD data in Liu et al 2009, 2011? Could this cdf-matching improve the soil moisture merging within ESA CCI? The authors could perhaps elaborate on this, to better motivate the approach.

Yes, this is a general purpose method that can be used in similar situations. The the code will be included in https://github.com/TUW-GEO/pytesmo in the future. We are right now (literally) evaluating this method in the ESA CCI SM product.

We will add a sentence to the manuscript mentioning the general usability of the method:

[8 : 22] We propose here improvements to this method to derive more robust scaling parameters that are not specific to VOD data but rather should be generally applicable in similar situations.

16. Page 10, line 11. Does this happen very often? Could this be one aspect to improve to increase coverage?

A fraction in the order of $1/10^6$ to $1/10^8$ of values are lost this way, so only very little temporal coverage increase is to be gained here.

Added:

[10 : 11] These values are deemed unreliable and are removed. However, this occurs very rarely, only a fraction of about $1/10^6$ to $1/10^8$ of values are lost in this way.

17. Page 10, line 18. Have the authors tried with the median statistic? It is less sensitive to ouliers.

No, we have not but this is a good idea. As it will only make a difference if three or more sensors have a value at a certain date, the expected change would be small. And since we already released the data as a requirement to submit a manuscript here, it likely would not make a difference big enough to warrant a new release of its own. As such we will evaluate this for the new version.

[11:12] Alternatively, one could also take the median instead of the mean. This would likely be more robust to outliers but would only make a difference if three or more concurrent values exist. As such the difference would likely be very small and

thus this is not explored in detail.

18. Figure 3. I do not think this Figure is necessary.

This Figure has been changed many times, we were never content with it. As also reviewer #1 finds it "actively confusing" and it is redundant with the text, we agree and will happily get rid of it.

19. Figure 4. What is the dominant vegetation in the chosen pixel? Perhaps the author could also include an example of time series in which TMI is also used, for completeness.

It is in Austria, mostly farmland, taking a look at google maps it is about 20% forest, also the Danube flows through it. We would rather reduce the number of Figures as we already have a lot of them. We like the current location because it shows a case where AMSR2 cannot directly be scaled to AMSR-E.

Updated first sentence of figure 4 caption:
Example X-band time series (15.125°E, 48.125°N in Austria, mostly farmland with about 20% forest cover) at (a) different processing steps and (b) violin plot showing the effect of CDF-matching on the distribution of VOD.

20. Page 12, line 3. The authors could also perhaps refer to the L-band VOD spatial patterns, which are consistent and correlate well with canopy height (e.g. Konings et al., L-band vegetation optical depth and effective scattering albedo estimation from SMAP, Remote Sensing of Environment, 2017).

[13:5] Similarly to previous findings based on L-band (Konings and Gentine, 2017), this figure also shows that on average VOD is highest in forests and lowest over bare ground.

21. Figure 6. It is hard to see the seasonal patterns. The authors could perhaps consider showing only the period 2002-2017 (or even shorter)

One of the main purposes of this Figure is to illustrate the temporal and spatial extent of the different VODCA products. Therefore we show the full temporal coverage.

22. Page 15, line 1. It is unclear how the authors measure the spatio-temporal coverage. Is Fig. 8 showing the fraction of days each month as stated in the label? The final temporal resolution shown in the Figure and referenced in the text above is unclear.

We agree, the sentences describing the calculation were a bit convoluted. The calculation for each month and latitude is: "number of observations of all pixels of a latitude" / ("number of land pixels of a latiude" x "number of days in month").

We reworked the label to figure 8:
Hovmoeller diagrams showing for each latitude and month the fraction of days per month with observations. The number of observations of a latitude and month are counted and then divided by the number of days per month and the number of land grid points at that latitude.

23. Page 15, line 14. What do the authors understand by a “CDF-matching failure”? could it be for one specific reason (e.g. see comment #15 above), or several? please,be more specific.

CDF matching fails if not enough AMSR-E data is available to retrieve robust scaling parameters. The rules are explained in detail in section 3.2.4, "Practical implementation and exceptions". We agree that not having a reference here to that subsection makes it hard for a reader to retrieve that information.

We will summarize the reason shortly together with a reference to section "Practical implementation and exceptions" in page 15, line 14.

24. Page 19, line 29. This advice is helpful but it could really be useful and applicable if converted into a criteria that contributes to a quality flag. There is clearly a need for a quality flag.

This is already included as a quality flag (bit-flag: 11), but we did not mention it in the text. Currently it is only described in the methods, page 10, line 6-7 ("The published data sets contain a flag indicating the matching method, allowing the user to remove the AMSR2 observations matched directly to AMSR-E if desired."

To make it clearer, we will mention the existence of this flag again on page 19, line 29. Also, as already previously mentioned, we will add a section to the appendix listing all flags, their meaning and their effects on the data quality.

25. Fig. 12. I would suggest to include subfigures f and g into a separate Figure, for clarity.

We concur, separating them by time span makes it clearer. We separated them.

26. Page 21, line 17. Only Ku band spans three decades, this sentence is a bit misleading.

True, this is not precise. How about:

[21 : 17] We present to the scientific community VODCA, three long-term VOD data sets spanning up to three decades that can be used to study dynamics in the biosphere.

27. Page 21, line 21. From section 4.2., it is unclear that the resulting VOD data sets provide observations "on a daily basis".

Agreed, better to describe actual temporal coverage and not base sampling frequency. How about:

[21 : 21] ... with the added benefit of having observations unaffected by cloud cover, allowing generally for more than 40% of days having a valid VOD value.

28. Page 21, line 24. The authors could perhaps consider mentioning at some point in the manuscript that their work is particularly relevant in the context of the prospect launch of the multi-frequency candidate mission Copernicus Microwave Imaging Radiometer (CIMR, www.cimr.eu)

While we agree with the sentiment, this would only fit in if we would have already talked about this extensively in a previous section. Each other sentence is summarizing a (sub)section, so even if we would mention CIMR before it would still not fit in the conclusions.

References

Chaparro, D., Piles, M., Vall-llossera, M., Camps, A., Konings, A. G., and Entekhabi, D.: L-band vegetation optical depth seasonal metrics for crop yield assessment, Remote Sensing of Environment, 212, 249–259, https://doi.org/10.1016/J.RSE.2018.04.049, https://www.sciencedirect.com/science/article/pii/S0034425718302062{#}bb0240, 2018.

Dorigo, W., Gruber, A., De Jeu, R., Wagner, W., Stacke, T., Loew, A., Albergel, C., Brocca, L., Chung, D., Parinussa, R., and Kidd, R.: Evaluation of the ESA CCI soil moisture product using ground-based observations, Remote Sensing of Environment, 162, 380–395, https://doi.org/10.1016/J.RSE.2014.07.023, https://www.sciencedirect.com/science/article/pii/S0034425714002727?via{%}3Dihub{#}f0045, 2015.

Fan, L., Wigneron, J.-P., Xiao, Q., Al-Yaari, A., Wen, J., Martin-StPaul, N., Dupuy, J.-L., Pimont, F., Al Bitar, A., Fernandez-Moran, R., and Kerr, Y.: Evaluation of microwave remote sensing for monitoring live fuel moisture content in the Mediterranean region, Remote Sensing of Environment, 205, 210–223, https://doi.org/10.1016/J.RSE.2017.11.020, https://www.sciencedirect.com/science/article/pii/S0034425717305692, 2018.

Green, S. B.: How Many Subjects Does It Take To Do A Regression Analysis, Multivariate Behavioral Research, 26, 499–510, https://doi.org/10.1207/s15327906mbr2603_7, http://www.tandfonline.com/doi/abs/10.1207/s15327906mbr2603{_}7, 1991.

Kerr, Y. H., Wigneron, J.-P., Al Bitar, A., Al-Yaari, A., Kaminski, T., Richaume, P., Mermoz, S., Rodríguez-Fernández, N. J., Mialon, A., Le Toan, T., Bouvet, A., and Brandt, M.: An evaluation of SMOS L-band vegetation optical depth (L-VOD) data sets: high sensitivity of L-VOD to above-ground biomass in Africa, Biogeosciences, 15, 4627–4645, https://doi.org/10.5194/bg-15-4627-2018, 2018.

Konings, A. G., Rao, K., and Steele-Dunne, S. C.: Macro to micro: microwave remote sensing of plant water content for physiology and ecology, New Phytologist, 223, nph.15 808, https://doi.org/10.1111/nph.15808, https://onlinelibrary.wiley.com/doi/abs/10.1111/nph.15808, 2019.

Liu, Y. Y., van Dijk, A. I. J. M., de Jeu, R. A. M., and Holmes, T. R. H.: An analysis of spatiotemporal variations of soil and vegetation moisture from a 29-year satellite-derived data set over mainland Australia, Water Resources Research, 45, https://doi.org/10.1029/2008WR007187, http://doi.wiley.com/10.1029/2008WR007187, 2009.

Owe, M., de Jeu, R., and Walker, J.: A methodology for surface soil moisture and vegetation optical depth retrieval using the microwave polarization difference index, IEEE Transactions on Geoscience and Remote Sensing, 39, 1643–1654, https://doi.org/10.1109/36.942542, http://ieeexplore.ieee.org/document/942542/, 2001.

Owe, M., de Jeu, R., and Holmes, T.: Multisensor historical climatology of satellite-derived global land surface moisture, Journal of Geophysical Research, 113, F01 002, https://doi.org/10.1029/2007JF000769, http://doi.wiley.com/10.1029/2007JF000769, 2008.

Sawada, Y., Tsutsui, H., Koike, T., Rasmy, M., Seto, R., and Fujii, H.: A field verification of an algorithm for retrieving vegetation water content from passive microwave observations, IEEE Transactions on Geoscience and Remote Sensing, 54, 2082–2095, https://doi.org/10.1109/TGRS.2015.2495365, http://ieeexplore.ieee.org/document/7331296/, 2016.

Tian, F., Wigneron, J.-P., Ciais, P., Chave, J., Ogée, J., Peñuelas, J., Ræbild, A., Domec, J.-C., Tong, X., Brandt, M., Mialon, A., Rodriguez-Fernandez, N., Tagesson, T., Al-Yaari, A., Kerr, Y., Chen, C., Myneni, R. B., Zhang, W., Ardö, J., and Fensholt, R.: Coupling of ecosystem-scale plant water storage and leaf phenology observed by satellite, Nature Ecology & Evolution, 2, 1428–1435, https://doi.org/10.1038/s41559-018-0630-3, http://www.nature.com/articles/s41559-018-0630-3, 2018.

Vreugdenhil, M., Hahn, S., Melzer, T., BauerMarschallinger, B., Reimer, C., Dorigo, W. A., and Wagner, W.: Assessing Vegetation Dynamics Over Mainland Australia With Metop ASCAT, IEEE Journal of Selected Topics in Applied Earth Observations and Remote Sensing, 10, 2240–2248, https://doi.org/10.1109/JSTARS.2016.2618838, http://ieeexplore.ieee.org/document/7762756/, 2017.

Main changes to: The Global Long-term Microwave Vegetation Optical Depth Climate Archive VODCA

Leander Moesinger[1], Wouter Dorigo[1], Richard de Jeu[2], Robin van der Schalie[2], Tracy Scanlon[1], Irene Teubner[1], and Matthias Forkel[1]

[1]Vienna University of Technology, Department of Geodesy and Geoinformation, Gußhausstraße 27-29, 1040 Vienna, Austria
[2]VanderSat, Wilhelminastraat 43A, 2011 VK Haarlem, The Netherlands

Correspondence: Leander Moesinger (Leander.Moesinger@geo.tuwien.ac.at, vodca@geo.tuwien.ac.at)

The main changes to the manuscript are as follows:

- Reworked large parts of abstract and introduction to make them more concise.
- Shortened the introduction to remove redundant text that repeated the abstract.
- Used Liu's VOD (section 2.2.1) to assess the quality of VODCA (section 4.4.1) and to see whether the studies performed with LiuVOD would have gotten similar results as with VODCA (section 4.4.2 and added LiuVOD to hovmoeller plots).
- Added a stability analysis to check if temporal dynamics of VODCA stay constant over time (section 4.1)
- Added a discussion about the absence of L-band (section 5.4).
- Added short brief discussion about merging different observation times, spatial footprints, incidence angles (section 5.5)
- Updated the look of many figures to improve their readability and make the look nicer.
- Added summary of quality flags and description of variables in data to supplement.

Other than that there are numerous minor changes, mostly in response to the reviewers comments.

The Global Long-term Microwave Vegetation Optical Depth Climate Archive VODCA

Leander Moesinger[1], Wouter Dorigo[1], Richard de Jeu[2], Robin van der Schalie[2], Tracy Scanlon[1], Irene Teubner[1], and Matthias Forkel[1]

[1]Technische Universität Wien, Department of Geodesy and Geoinformation, Gußhausstraße 27-29, 1040 Vienna, Austria
[2]VanderSat, Wilhelminastraat 43A, 2011 VK Haarlem, The Netherlands

Correspondence: Leander Moesinger (Leander.Moesinger@geo.tuwien.ac.at, vodca@geo.tuwien.ac.at)

Abstract. Since the late 1970s, spaceborne microwave ~~sensors~~ radiometers have been providing measurements of radiation emitted by the Earth's surface. From these measurements it is possible to derive vegetation optical depth (VOD), a model-based indicator related to ~~vegetation densityand its relative water content~~ the density, biomass, and water content of vegetation. Because of its high temporal resolution and long availability, VOD can be used to monitor short- to long-term changes in vegetation. However, studying long-term VOD dynamics is generally hampered by the relatively short time span covered by the individual microwave sensors. This can potentially be overcome by merging multiple VOD products into a single climate data record. ~~But~~However, combining multiple sensors into a single product is challenging as systematic differences between input products ~~, e.g.~~ like biases, different temporal and spatial resolutions and coverage ~~,~~need to be overcome.

Here, we present a new series of long-term VOD products, ~~which combine multiple VOD data sets derived from several~~ the VOD Climate Archive (VODCA). VODCA combines VOD retrievals that have been derived from multiple sensors (SSM/I, TMI, AMSR-E, Windsat ~~,~~and AMSR-2) using the Land Parameter Retrieval Model. We produce separate VOD products for microwave observations in different spectral bands, namely Ku-band (period 1987-2017), X-band (1997-2018) ~~,~~and C-band (2002-2018). In this way, our multi-band VOD products preserve the unique characteristics of each frequency with respect to the structural elements of the canopy. Our ~~approach to merge the single-sensor VOD products is similar to the one of the ESA CCI Soil Moisture products (Liu et al., 2012; Dorigo et al., 2017)~~merging approach builds on an existing approach that is used to merge satellite products of surface soil moisture: First, the data sets are co-calibrated via cumulative distribution function matching using AMSR-E as scaling reference. ~~We~~ To do so, we apply a new matching technique that scales outliers more robustly than ordinary piece-wise linear interpolation. Second, we aggregate the data sets by taking the arithmetic mean between temporally overlapping observations of the scaled data~~, generating a VOD Climate Archive (VODCA)~~.

The characteristics of VODCA are assessed for self-consistency and against other products~~: spatio-temporal~~ . Using an autocorrelation analysis, we show that the merging of the multiple data sets successfully reduces the random error compared to the input data sets. Spatio-temporal patterns and anomalies of the merged products show consistency between frequencies and ~~both with observations of~~ with Leaf Area Index ~~derived~~ observations from the MODIS instrument as well as with Vegetation

Continuous Fields from the AVHRR instruments. ~~Trend analysis~~ Long-term trends in Ku-Band VODCA shows that since 1987 there has been a decline in VOD in the tropics and in large parts ~~parts~~ of east-central and north Asia~~along with a strong increase~~ , while a substantial increase is observed in India, large parts of Australia, south Africa, southeastern China and central north America. ~~Using an autocorrelation analysis, we show that the merging of the multiple data sets successfully reduces the random error compared to the input data sets.~~ In summary, VODCA shows vast potential for monitoring ~~spatio-temporal ecosystem behaviour complementary to~~ spatial-temporal ecosystem changes as it is sensitive to vegetation water content and unaffected by cloud cover or high sun zenith angles. As such it complements existing long-term ~~vegetation products from optical remote sensing~~optical indices of greenness and leaf area.

The VODCA products (Moesinger et al., 2019) are open access and available under Attribution 4.0 International at https://doi.org/10.5281/zenodo.2575599

1 Introduction

Vegetation attenuates microwave radiation that is emitted or reflected by the Earth surface. The degree of attenuation can be derived from passive and active microwave satellite observations and is commonly referred to as Vegetation ~~optical depth~~ Optical Depth (VOD) ~~(Jackson and Schmugge, 1991)~~(Jackson and Schmugge, 1991; Vreugdenhil et al., 2016). The amount of attenuation depends on various factors, e.g. the density~~and type~~ , type and water content of vegetation, and the wavelength of ~~observation~~ the sensor (Jackson and Schmugge, 1991; Owe et al., 2008). Short wavelengths experience a higher attenuation by vegetation (and hence relate to higher VOD values) than longer ones ~~(Liu et al., 2009; Owe et al., 2008)~~(Liu et al., 2009; Owe et al., 2008; . As a consequence, VOD estimates from long wavelengths ~~contain more information on~~ are generally more sensitive to deeper vegetation layers (e.g. ~~stems) than~~ stem biomass) while VOD estimates from short wavelengths ~~(Chaparro et al., 2018)~~are more sensitive to leaf moisture content (Chaparro et al., 2018; Tian et al., 2018; Fan et al., 2018; Konings et al., 2019). VOD increases with the Vegetation Water Content (VWC) (Jackson and Schmugge, 1991) and therefore ~~by extension~~ is related to the Above-Ground dry Biomass (AGB) (Liu et al., 2015) and its Relative Water Content (RWC) (Momen et al., 2017).

Satellite-derived VOD has a wide range of potential applications, including biomass monitoring (Liu et al., 2015; Brandt et al., 2018b), drought monitoring (Liu et al., 2018), phenology ~~analyzes (Jones et al., 2011) and fire risk management (Fan et al., 2018)~~ analyses (Jones et al., 2011) and estimating the likelihood of wildfire occurrence (Fan et al., 2018; Forkel et al., 2017, 2019) . VOD also correlates with various optical remote sensing indicators of ~~plant productivity, e.g., Gross Primary Production (GPP) (Teubner et al., 2018), Leaf Area Index (LAI) (Vreugdenhil et al., 2017),~~ vegetation greenness like Normalized Difference Vegetation Index (NDVI), Enhanced Vegetation Index, ~~and~~ Normalized Difference Water Index (Grant et al., 2016)~~.~~ ,

and Leaf Area Index (LAI) (Vreugdenhil et al., 2017) and hence also relates to plant productivity (Teubner et al., 2018, 2019) . VOD has some distinct advantages over optical vegetation indexes for vegetation monitoring, such as a slower saturation and the resulting higher sensitivity to high biomass ~~areas such as rain-forests (Liu et al., 2015) ,~~ (Liu et al., 2015) or the ability to be retrieved despite of cloud cover (Liu et al., 2011a) which are both advantageous for monitoring tropical forest regions (van Marle et al., 2016).

VOD products have been derived from multiple ~~spaceborne~~ space-borne microwave sensors that have been in orbit since the late 1970s (Owe et al., 2008). These sensors have varying lifetimes and characteristics, resulting, e.g., from differences in microwave frequency used, measurement incidence angles, orbit characteristics, radiometric quality, and spatial footprints. This complicates their joint use in studying long-term VOD dynamics. To overcome this issue, Liu et al. (2011a) proposed a long-term (1987-2008) ~~harmonised~~ harmonized multi-sensor VOD data set by merging VOD products derived from the Special Sensor Microwave/Imager (SSM/I), the Microwave Imager onboard the Tropical Rainfall Measuring Mission (TMI), and the Advanced Microwave Scanning Radiometer - Earth Observing System (AMSR-E) through the Land Parameter Retrieval Method (LPRM; Owe et al. (2008)). Their methodology was inherited from the methodology used to produce the first long-term satellite-based climate data record of soil moisture within the the Climate Change Initiative of the European Space Agency (ESA CCI Soil moisture; (Dorigo et al., 2017, 2012; Liu et al., 2011c, 2012; Gruber et al., 2019)). In their methodology, all available observations were ~~harmonised~~ harmonized with respect to C-Band (6.9 GHz) VOD observations from AMSR-E, which was assumed to provide the highest quality observations (Liu et al., 2012). Only in periods where AMSR-E C-band observations were not available, other products were used instead. This approach ignores the fact that in a statistical sense a ~~high quality~~ high-quality product can be fused with a ~~low quality~~ low-quality product to create a product with a higher quality than either of the original products. This was systematically demonstrated for the merging of two level 2 soil moisture products (Gruber et al., 2017). Since the release of the multi-satellite VOD product by Liu et al. (2011a), significant progress has been made towards a better understanding of the VOD signal~~, and it~~ . It was shown that also the individual bands carry valuable information for different applications (Teubner et al., 2018; Chaparro et al., 2018), which ~~prompts the generation of~~ demonstrates the need for frequency-specific VOD data sets. In addition, new sensors ~~have been~~ were launched, allowing the observational VOD records to be extended to the running present.

In this paper, we present a new series of long-term, ~~harmonised~~ harmonized VOD climate data records, called the VOD Climate Archive (VODCA), which are derived from multiple single-sensor level 2 products. ~~Our data sets use~~ VODCA uses a similar core methodology as in Liu et al. (2011a) and in ESA CCI Soil Moisture ~~but significantly progresses the current state-of-the-art, based on the~~ (Gruber et al., 2019) but incorporates the latest insights on VOD and climate data record production gathered during the last few years, and ~~by introducing~~ introduces recent satellite missions. We combine VOD observations from SSM/I, TMI, AMSR-E, WindSat, AMSR2 into global, harmonised long-term VOD products at a 0.25° spatial sampling and covering the period 1987-2018. ~~Similar to the approach of Liu et al. (2011a), we use Cumulative Distribtion Function (CDF) matching techniques to scale all VOD data sets to the distribution of AMSR-E. However, since VOD is a function of~~

~~the frequency and, consequently, different canopy information is stored in different bands, we do not amalgamate all bands but instead produce three individual products: one for Ku-band, one for X-band, and one for C-band. Even though VOD products also exist in L-band derived from the sensors SMAP and SMOS, preliminary analysis concluded that their short overlapping time span and low temporal correlation between them do not warrant a product for it. Also, we discuss the susceptibleness of piece-wise linear CDF-matching to extreme values and as solution propose a new hybrid CDF-matching technique that scales very high and very low values more robustly. Besides, in contrast to Liu et al. (2011a) we merge the scaled observations by taking the arithmetic mean whenever more than one observation is available. From a statistical perspective this should lead to data sets with reduced random error compared to the input products.~~First, we describe the input VOD data sets, followed by an overview of the fusion methodology. We then describe the main characteristics of the merged data sets in terms of spatial and temporal coverage and patterns, and their random error characteristics. ~~The~~ We check the spatio-temporal characteristics ~~are checked~~ for plausibility by comparing them to those of related satellited-derived biogeophysical products ~~, e.g. Vegetation Continuous Fields (VCF) and LAI. We~~ and complement the data set assessment by a trend analysis. ~~The assessment will be concluded with the~~ We conclude the paper with a discussion on current limitations and ways forward.

2 Input data

2.1 VOD data sets

2.1.1 The land-parameter retrieval model (LPRM)

LPRM v6 (van der Schalie et al., 2017; Owe et al., 2008; Meesters et al., 2005) is based on a radiative transfer model first proposed by Mo et al. (1982) and simultaneously retrieves soil moisture and VOD ~~at the same time~~ from vertical and horizontal polarized microwave data~~and is based on a radiative transfer model (Mo et al., 1982)~~. The model assumes that the earth emits microwave radiation depending on its surface temperature T_s and emissivity e which is a function of its dielectric constant k, which in turn is dependent on the surface soil moisture. Part of this radiation is then absorbed or scattered by water in the vegetation depending on its transmissivity Γ and single scattering albedo w while the vegetation itself also emits radiation depending on its temperature T_v. The resulting brightness temperature T_b measured at the sensor can then be modeled as

$$T_{bp} = T_s e_p \Gamma + (1-\Gamma) T_v (1-w) + (1-e_p)(1-w) T_v (1-\Gamma)\Gamma \quad (1)$$

where the subscript p denotes either a vertical or horizontal polarization. Further, VOD (τ) is related to Γ and the incidence angle u by:

$$\Gamma = \exp\left(\frac{-\tau}{\cos(u)}\right) \quad (2)$$

Since observations from the sensors used in this study are available in both horizontal and vertical polarization, eq. 1 is used to open a system of linear equations. While the the absolute measured T_{bH} is lower than T_{bV}, it is more sensitive to changes in soil moisture while T_{bV} is more sensitive to vegetation and surface soil temperature. This relationship in combination with

the application of a separate retrieval algorithm to determine the temperature from 37-GHz vertical polarization measurements (Holmes et al., 2009) allows to solve the system analytically as described in Meesters et al. (2005).

The actual temperatures are difficult to estimate during daytime due to surface heating, while during nighttime, soil and vegetation are ~~in a near~~ nearly in thermal equilibrium. This implies that nighttime retrievals are expected to have a lower temperature-related error than daytime retrievals (Owe et al., 2008). Therefore, to minimize error sources, only nighttime retrievals are used in VODCA. While LPRM v6 is not publicly available, older versions are available trough GFSC: https://disc.gsfc.nasa.gov/datasets/LPRM_AMSR2_D_SOILM3_001/summary

2.1.2 Sensor specifications

The used VOD data sets were derived from brightness temperature measurements of various ~~spaceborne~~ space-borne sensors active since 1987 (Fig. 1).

The Advanced Microwave Scanning Radiometer (AMSR-E) onboard ~~AQUA~~ Aqua retrieved microwave observations from 2002 to 2011 in six bands, of which we only consider the C-, X-, and Ku-band. Their spatial footprint is 75×43 km, 51×29 km and 27×16 km respectively. AQUA is on an sun-synchronous circular orbit, passing the equator at 1:30 PM ascending and 1:30 AM descending mode (Knowles et al., 2006; Kawanishi et al., 2003).

The Advanced Microwave Scanning Radiometer 2 (AMSR2) is an improved version of AMSR-E onboard GCOM-W1 continuing AMSR-E's measurements since 2012 with similar bands, orbit and overpass times but with a slightly higher spatial resolution: 62×35 km, 42×24 km and 22×14 km, for C-, X-, and Ku-band respectively. In addition, AMSR2 also contains a second C-band (7.3 GHz) that can be used to cover areas where ~~RFI~~ Radio-Frequency Interference (RFI) is present in the primary C-band channel (6.9 GHz) (Meier et al., 2018). During preliminary analysis, we discovered that the AMSR2 Ku-band VOD retrievals have an apparent break in late 2017. Since then, the values observed are globally systematically lower than before, indicating possibly a calibration error in Ku-band brightness temperatures. While the exact reasons are unknown to us, until the matter is resolved we do not include Ku-band data after 2017-08-01 into VODCA. This shortens the Ku-band VOD product by 16 months. VOD retrievals from X- and C-band AMSR2 seem unaffected and are used until the end of 2018.

The Special Sensor Microwave Imager (SSM/I) is onboard a series of DMSP satellites. We use the VOD data retrieved from F-8, F-11 and F-13. From the 7 available bands of SSM/I we use only VODfrom Ku-band which has a resolution of 69×43 km. The equatorial crossing time varies between the DMSP satellites, but all are on sun-synchronous orbits (Wentz, 1997).

Among other sensors, the Tropical Rainfall Measuring Mission (TRMM) carried the TRMM Microwave Imager (TMI). TRMM is the only satellite used which has a non-near-polar orbit with an inclination of 35 degrees. Up to 2001 it had an altitude of 350 km, which then got boosted to 400 km leading to a slight decrease in spatial resolution. TMI was active from

1997 to 2015. Of the 9 channels we only use its X- and Ku-band, which ~~has~~ have a spatial resolution of 63×37 km / 72×43 km and 30×18 km / 35×21 km pre/post boost, respectively (Kummerow et al., 1998).

WindSat onboard Coriolis was launched in 2003 on a sun-synchronous orbit providing radiometric measurements in five bands, of which the C-, X- and Ku-band were used to derive VOD. The spatial resolution is 39×71 km, 25×38 km and 16×27 km. Due to some periods of non-operation, WindSat contains temporal data gaps (Gaiser et al., 2004). Unfortunately we were unable to gain access to data past July 2012, even though WindSat is still operational.

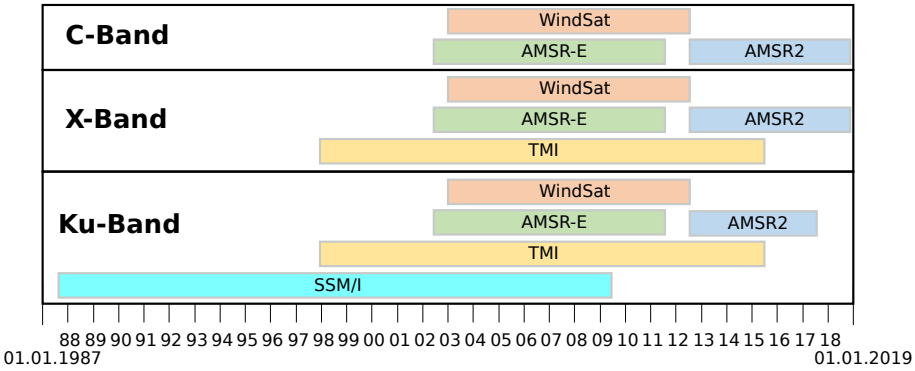

Figure 1. Time periods of the sensors used for each band.

Table 1. The input VOD data sets used with their temporal coverage, local ascending equatorial crossing times (AETC) and used frequencies [GHz] for each product.

Sensor	Time period used	AECT	C-Band	X-Band	Ku-Band	Reference
AMSR-E	Jun 2002 - Oct 2011	13:30	6.93	10.65	18.7	van der Schalie et al. (2017)
AMSR2	Jul 2012 - Jan 2019	13:30	6.93 & 7.3	10.65	18.7	van der Schalie et al. (2017)
SSM/I F08	Jul 1987 - Dec 1991	18:15			19.35	Owe et al. (2008)
SSM/I F11	Dec 1991 - May 1995	17:00 - 18:15		19.35	Owe et al. (2008)	
SSM/I F13	May 1995 - Apr 2009	17:45 - 18:40		19.35	Owe et al. (2008)	
TMI	Dec 1997 - Apr 2015	Asynchronous		10.65	19.35	Owe et al. (2008)
WindSat	Feb 2003 - Jul 2012	18:00	6.8	10.7	18.7	Owe et al. (2008)

2.2 Evaluation data

2.2.1 Liu et al. VOD

We compared the VODCA datasets with the previously created multi-sensor, multi-band VOD dataset (Liu et al., 2011b, 2015) , hereafter called LiuVOD. LiuVOD covers the period January 1993 to December 2012 and is based on VOD retrieved via LPRM from SSM/I (Ku-band), TMI (X-band), and AMSR-E (C/X-Band) observations. The values are scaled to AMSR-E and methods are in place to fill gaps due to frozen ground and to correct for large-scale open water bodies. We expect that the data that are publicly available were subject to some temporal smoothing since the data are mostly gap-free. Unfortunately, we could find no mention of this in either of the two papers and their supplementary information.

2.2.2 MODIS leaf area index

To ~~vertify~~ verify the plausibility of VODCA we compare it to MODIS leaf area index (LAI), MOD15A2H version 6 (Myneni et al., 2015). LAI is the ~~one-sided ratio of~~ ratio of one-sided leaf area to ground area and is estimated from the ~~red and NIR MODIS data~~ solar-reflective MODIS bands using a look-up-table based approach with a back-up algorithm that uses empirical relationships between NDVI, LAI and fraction of photosynthetically active radiation (FPAR). Field studies with different crop types showed that VOD is closely related to LAI (Sawada et al., 2016), a relationship that has been already used to assess VOD products derived from active sensors (Vreugdenhil et al., 2017). The data is available globally since 2002 with an 8-day temporal resolution, and is for comparison purposes spatially downsampled from its native resolution of 500 metres to a quarter degree grid. The original data are available on https://lpdaac.usgs.gov/data_access/data_pool .

2.2.3 AVHRR vegetation continuous fields

We ~~us~~ use the vegetation continuous fields (VCF) version 1 ~~by Hansen and Song (2018); Song et al. (2018) which show~~ derived from data of Advanced Very High Resolution Radiometer (AVHRR) instruments (Hansen and Song, 2018; Song et al., 2018) . The VCF product shows the fractional cover of bare ground, short vegetation and tree canopy, where trees are defined as all vegetation taller than 5 metres in height and short vegetation ~~all shorter vegetation . They produced~~ is defined as vegetation smaller than 5 metres. VCFs are provided as yearly files from 1982 to 2016 indicating the fractional coverage during the local annual peak of growing season. The VCF ~~are derived from data of Advanced Very High Resolution Radiometer (AVHRR) instruments~~ product is distributed by the Land Long Term Data Record (LTDR) ~~project~~ at https://search.earthdata.nasa.gov

Given the relation of ~~vegetation height (Lefsky et al., 2005) and VOD to biomass~~ VOD with vegetation height and biomass Giardina et al. (2018); Liu et al. (2015), it seems sensible to assume that VOD would ~~be highest / medium / lowest in areas with high tree canopy / short vegetation / bare ground coverage, respectively. We~~ increase from areas with bare ground and short vegetation to areas with high tree cover. Hence, we use the VCF data ~~for two purposes. First (sec. 4.1), we~~ to calculate the mean VCF from 2002 to 2016 and compare it to the mean of the VODCA products from 2002-2017 ~~. Second~~ (sec. ~~4.4.2)~~4.1). Furthermore, we calculate the VCF trends from 1987 to 2016 and compare it to the trends in the merged Ku-band VOD ~~of the same time period to spot differences in trends~~over the same period (sec. 4.4.2). Song et al. (2018) also calculated ~~and distributed~~ VCF trends by first determining whether there is a significant ~~trends~~ trend with a Mann-Kendall test and then calculating the slope with a Theil-Sen estimator. Both are non-parametric tests that are robust to outliers, but using different methods to mask

for significance and estimate the slope can lead to significant slopes that are still very small. To ~~alleviate the~~ avoid this issue, we ~~too~~ also calculate the slope using a Theil-Sen estimator ~~, but we~~ and use the Theil-Sen estimator ~~also~~ to determine a 95% confidence interval for the slope and remove any slopes where the zero-slope is within the confidence interval.

3 Methods

~~The~~ For each of the VODCA products, we use almost exactly the same methodology~~is used for the product of each~~. Exceptions to this common methodology are described at the end of the respective subsection. Each product is computed without any influence of the others~~, with exceptions being described at the end of the respective section~~. The main difference between the three products is the time period spanned~~by each product~~, resulting from the varying availability of input data (Fig. 1). The fusion process involves three main processing steps~~.~~: First, preprocessing involves masking for spurious observations and spatial and temporal collocation of the data sets. Second, bias between the different sensors is ~~corrected for~~ removed by scaling them to ~~the VOD climatology of~~ AMSR-E ~~C-, X-, and Ku-band, respectively~~VOD. Ultimately, the collocated and bias-corrected observations of all data sets are merged in time and space.

3.1 Preprocessing

Level 2 VOD data in swath geometry were first projected onto a common regular $0.25° \times 0.25°$ latitude-longitude grid using nearest neighbour resampling. The different sensors visit the same spot on the Earth surface at different times of the day. To facilitate further processing, ~~all observations are temporally resampled to UTC midnight. This is done as in ESA CCI soil moisture (Dorigo et al., 2017) by taking for every 0:00 UTC the closest observation~~ we do not take into account the exact time of observation. Instead, we selected for every UTC midnight the closest nighttime value in a window of ± 12 hours ~~if any is available~~which is identically as in the ESA CCI soil moisture processor (Dorigo et al., 2017). Since in subsequent processing steps the values of different sensors with different measurement times will be merged, one can consider the resulting values as nightly averages.

Basic masking operations were applied to remove potentially spurious observations. Specifically we mask for ~~radio frequency interference (RFI)~~RFI, low land surface temperatures (LST), and VOD values ≤ 0 as follows:

- RFI: Artificial microwave emitters on the Earth's surface distort the signal received by the satellite, causing the resulting VOD values at those locations to be unreliable. RFI is typically frequency-specific. RFI flags were already provided with the level 2 VOD data and were based on de Nijs et al. (2015). Any observations affected by RFI are removed.

- LST: Due to the different dielectric properties of ice and water, reliable retrievals can only be made if the ground is not frozen. Therefore, we remove observations where the LST is below 0° C. Masking for LST was based on the temperature retrievals of from Ka-band (Holmes et al., 2009), which is found on all the multi-channel instruments used in VODCA, and were provided with the level 2 VOD data.

– Negative VOD values: VOD retrievals <0 are physically impossible and are therefore removed from the data sets. We also remove VOD values of 0.0 (floating point zero). The reasoning is twofold: First, it is physically only possible to get floating point zero VOD if there is virtually no vegetation, making it very unlikely for most parts of the globe. Second, we observed that this case occurs surprisingly often ~~,~~ also in non-desert regions, and that these values never fitted well with the other observations. This indicates that most VOD values of zero are artifacts that have to be removed.

The above masking is applied independently to all sensors and bands. A special case is AMSR2, which has two channels in C-band, i.e. at 6.9 and 7.3 GHz. If possible, the observations from the 6.9 GHz band are used, but if the observation in this channel is masked, the 7.3 GHz observation is used instead (if unmasked) to fill gaps. This only causes a minor reduction in quality, as the two C-bands are strongly correlated (Supplementary Figure 1). A flag indicating the channel ultimately used in the merged data set for each observation is provided in the metadata.

3.2 Cumulative distribution function (CDF) matching

We use a new implementation of the CDF-matching technique ~~,~~ based on a combination of piece-wise linear interpolation and linear least squares regression. CDF-matching is used to correct for systematic differences between the VOD values of each sensor, which may result ~~,~~ e.g. ~~,~~ from the individual sensor designs, incidence angles, spatial footprints and the slight differences in the frequencies used. The goal of CDF-matching is to scale a source data set such that its empirical CDF becomes similar to the empirical CDF of the reference data set. CDF-matching is applied on a per-pixel basis and has been successfully used for similar tasks that require the correction of higher order differences between data sets (Liu et al., 2009, 2011a, 2012; Dorigo et al., 2017).

3.2.1 Ordinary piece-wise linear CDF-matching

Piece-wise linear CDF-matching (Liu et al., 2009, 2011a; Dorigo et al., 2017) predicts for each [0, 5, 10, 20, 30, ... , 80, 90, 95, 100] percentile of the source data the same percentile of the reference data set. Values between the n^{th} and n^{th}+1 percentile are then scaled using linear interpolation. While the scaling parameters are determined only from temporally overlapping observations, during prediction there can be values outside the training range. These values are scaled by extrapolating the first or last percentile interval. This method preserves the ranks of the source and computes rather fast. However, the first and last percentiles are defined by the lowest and highest observations, respectively, in both source and reference time series. Hence, a single outlier can greatly affect the parameters of these percentiles, making them unreliable. We propose here improvements to this method to derive more robust scaling parameters that are mot specific to VOD data but rather should be generally applicable in similar situations.

3.2.2 Improvements

We improved the original method by fitting a linear model using the sorted observations smaller than the second percentile with an intercept through the second percentile. This gives more reliable scaling parameters for low values since all the data between the lowest and second-lowest percentiles are used instead of just the lowest value. In case a different number of observations exists in the source and reference, the data with less observations is padded by linear interpolation during training. In a similar fashion, a model is fitted for observations above the penultimate percentile.

We further increase the robustness of the CDF-matching parameters by dynamically increasing the step size of the percentiles if only few observations are available. The number of observations varies greatly from grid point to grid point and from sensor to sensor. If too few observations exist between two subsequent matching-percentiles (a "bin"), the CDF-matching may overfit, leading to unreliable parameters. To counteract this, we dynamically reduce the number of bins and increase the size of the bins based on the number of observations.

3.2.3 Stability of parameters

To evaluate whether the new matching technique is more robust to outliers than the original piecewise linear ~~edf~~ CDF matching method, we simulate the variances of the derived parameters of each bin for a varying number of training observations using artificial values. The use of artificial values allows us to test the method without being influenced by the artifacts inherent to real data. To achieve this, we sample a set of source and reference values from a standard normal distribution, and then determine the resulting CDF-matching parameters. For each evenly spaced percentile bin, we determine the slope in radians. This is repeated a few thousand times for various numbers of values (representing time series with a varying number of observations), each time drawing new values. If a CDF-matching method is robust, the determined slopes should have low variance due to the values always being drawn from the same distribution.

We run this both with piece-wise linear CDF-matching and our new method. However, for this simulation we do not dynamically decrease the number of bins, as we are solely interested in the performance of the linear regression scaling the first and last percentile. Both methods are tested with the same randomly drawn data.

The resulting variances in the slope, for each percentile bin, for both methods, depend on the number of observations used for the parameter determination. This is shown in Fig. 2. The results in the middle bins are exactly the same, as the same methodology in used for these bins. However, in the case of linear piece-wise interpolation, the slope parameters of the first and last bins have a much higher variance than the middle bins as they are affected by outliers. In contrast, the slopes determined by the least-squares method have a much lower variance. In both cases we can also see that the more observations we have, the lower the variance of the slope parameter is, showcasing the reasoning behind reducing the number of bins dynamically if too few observations are available.

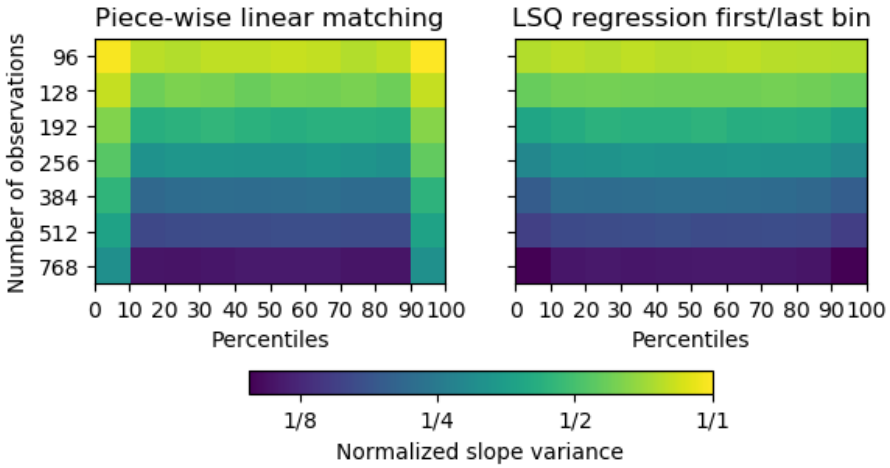

Figure 2. Variance of the derived slope, depending on the number of observations and the percentile bin for both piece-wise linear CDF-matching techniques. The color is log normalized.

3.2.4 Practical implementation and exceptions

While there is no "true" reference to scale to, AMSR-E has almost global coverage and has a long temporal overlap with all other sensors but AMSR2. Hence, the empirical CDFs of WindSat, TMI and SSM/I are directly scaled to the one of AMSR-E, similar to Dorigo et al. (2015). To preserve any potential trends in both source and reference data, only dates when both have a valid observation are used. If at a certain location less than 20 temporal overlapping observations exist, no reliable scaling parameters can be determined and the source time series is dropped. A bin size of 20 was chosen as compromise between data coverage and often used bin sizes. A bin size of 50 observations is often used as a rule of thumb for univariate regression to get robust estimates (Green, 1991). However, our main goal was rather to prevent time series with very few observations from learning spurious scaling parameters and we also did not want to loose all time series with less than 50 values. As such 20 was chosen as a compromise.

AMSR2 does not share any temporal overlap with AMSR-E and therefore cannot be directly scaled based on overlapping observations. Instead, for X- and Ku-band, scaled observations of TMI can potentially be used to bridge this gap. This is done according to the following logic~~(Fig. ??)~~: If possible, AMSR2 is scaled to the rescaled TMI. Should there not be enough overlapping observations, the scaling parameters are determined from all observations of the first two years of AMSR2 and the last two years of AMSR-E. While this removes any potential trends in the first two years of the AMSR2 period, these trends are still assumed to be smaller than the removed bias. Last, if there are also not enough AMSR2 or AMSR-E observations available in those years, the whole AMSR2 time series is dropped. For C-band, which is not covered by TMI, the AMSR2 data are always matched directly to AMSR-E ~~following the approach above~~by using the last and first two years of both sensors. The published

data sets contain a flag indicating the matching method, allowing the user to remove the AMSR2 observations matched directly to AMSR-E if desired.

Since the scaling parameters are determined using only a subset of all observations, during prediction there can be values outside the training range. The regression is not forced to go through the origin, therefore if the predicted values can potentially be smaller than 0. These values are deemed unreliable and ~~removed.~~are removed. However, this occurs very rarely, only a fraction of about $1/10^6$ to $1/10^8$ of values are lost this way.

~~Pseudo-code showing the CDF-matching logic of AMSR2~~

3.3 Merging

For all bands, the CDF-matched time series of all individual sensors are merged into a single long continuous time series. For a certain pixel at a certain time step, three possible scenarios can occur:

1. If on a certain date no sensor has an observation, a data gap will result in the final product;
2. If only one sensor has an observation, the CDF-matched value will be directly integrated in the final product;
3. If multiple sensors have an observation on a certain date, their arithmetic mean is taken.

This means that the number of sensors contributing to each observation within a time series can vary greatly. For each observation in the final product there is a flag indicating which sensors have contributed to it. Although more sophisticated weighted merging methods based on least squares have been proposed to merge multiple satellite observations (Gruber et al., 2017, 2019), estimating these weights, i.e. indicators of the relative quality of the individual data sets, is a non-trivial task. This particularly applies to VOD, for which no appropriate independent reference data exist. However, in most cases, the arithmetic mean appears to be a robust approximation of optimal merging (Liu et al., 2012).
Alternatively, one could also take the median instead of the mean. This would likely be more robust to outliers but would only make a difference if three or more concurrent values exist and as such the difference would likely be very small.

4 Properties of the long-term VOD data sets

4.1 Spatial patterns and temporal dynamics

Figure 3 shows an example of X-band VOD time series in Austria at different stages of merging procedure together with MODIS LAI. The original VOD time series have visible systematic differences between each sensor. The CDF-matched VOD time series have been scaled to AMSR-E and visually do not show systematic differences between sensors. The statistical distributions of VOD from the sensors are similar after matching (Fig. 3 b). This example grid point is north of 38N and thus outside the spatial coverage of TMI, therefore AMSR2 has been scaled to AMSR-E directly using non-temporally overlapping

observations. The merged VOD time series shows comparable seasonal dynamics like LAI.

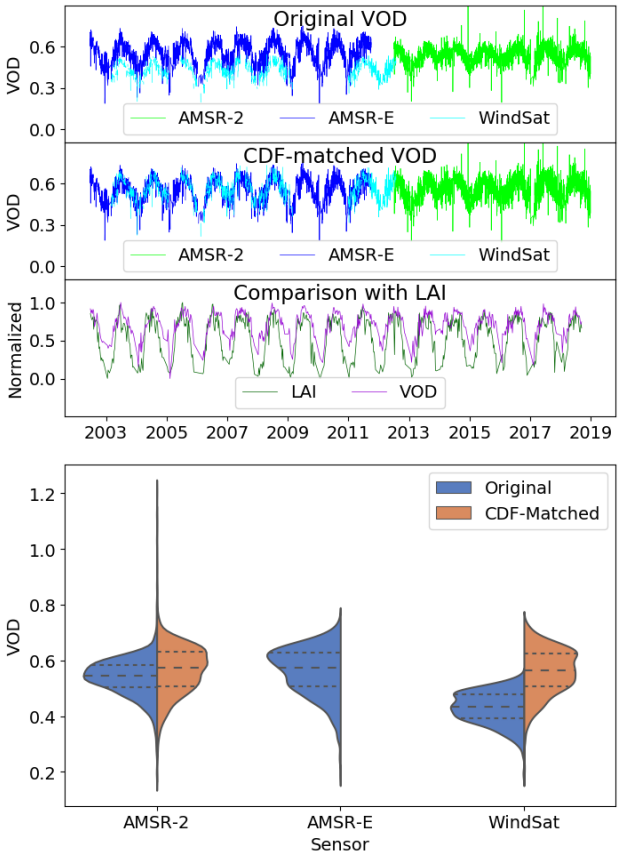

Figure 3. Top: Example X-band time series for a grid cell in Austria (~~lon / lat:~~ 15.125~~/~~ °E, 48.125°N, mostly farmland with about 20% forest) at different processing steps~~(a) and violin plot showing the effect of CDF-matching on its distribution (b)~~. Time series of the original VOD data of all available sensors ~~for that band at that location~~ are shown in the top panel, the CDF-matched series in the middle panel, and the final merged VOD (VODCA) is shown together with MODIS LAI in the bottom panel. In the bottom panel VOD and LAI are both normalized, VOD is downsampled by moving average to match the temporal 8-day resolution of LAI. Bottom: Violin plot showing the effect of CDF-matching on the statistical distribution of VOD.

The global spatial patterns of average VOD between June 2002 and June 2017 is shown for each band in Figure 4 (a-c). This period was selected because all bands have global coverage in this time period. All bands show similar spatial patterns, matching the ones of the VCF land covers (Fig. 4 (e), with high VOD in tropical and northern forests and lower VOD in grassland and desert regions. The same pattern is also visible in canopy height (Simard et al., 2011) and MODIS LAI (Fig. 4 (d), even though the LAI in the tropical forests is much higher than in the boreal forests, while VOD is similarly high in both regions. Based on the principle that the penetration of microwaves increases with wavelength, the maximum VOD is highest at

shorter wavelengths (Ku-band) and smallest at longer wavelengths (C-band). This can also be seen in Figure 4 (f) which shows the average VOD of each band for locations dominated by ~~TC, SV or BG, respectively. This~~ high tree cover (vegetation height > 5m), short vegetation (< 5m) or bare ground. Similarly to previous findings based on L-band (Konings and Gentine, 2017), this figure also shows that ~~as expected,~~ on average VOD is highest in forests and lowest over bare ground.

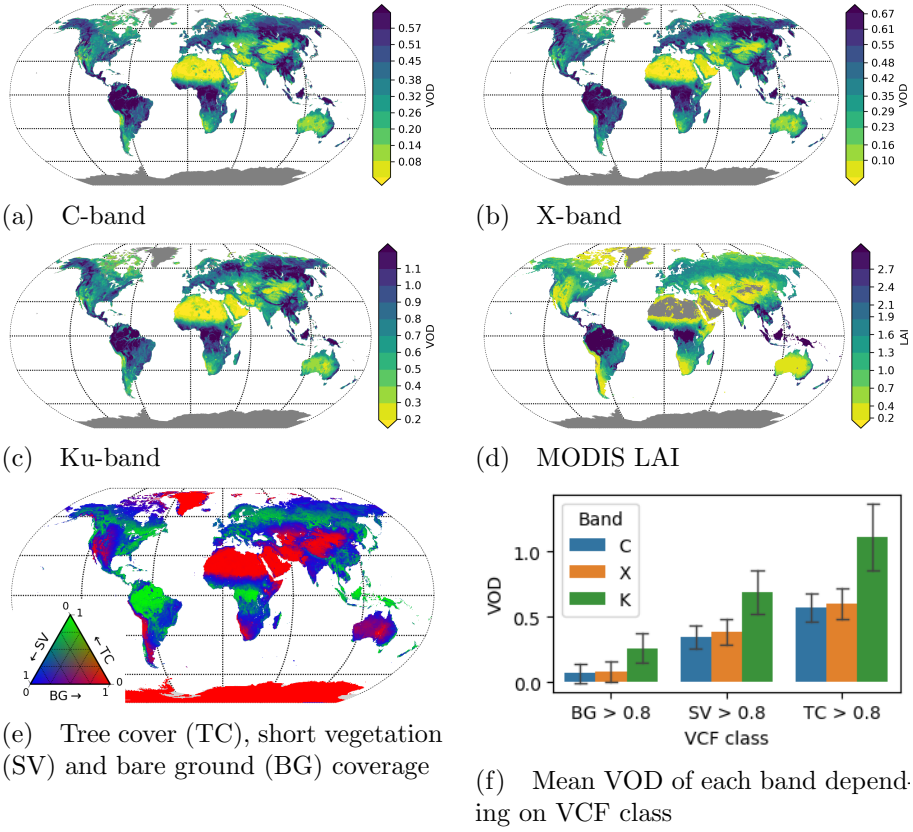

(a) C-band (b) X-band (c) Ku-band (d) MODIS LAI (e) Tree cover (TC), short vegetation (SV) and bare ground (BG) coverage (f) Mean VOD of each band depending on VCF class

Figure 4. Global spatial patterns of average multi-sensor VOD from each band (2002 to 2017), average MODIS LAI (2002 to 2017) and average VCF (~~2002 - 2016~~ 2002-2016 and distribution of VOD for locations with high tree cover (TC), short vegetation (SV) and bare ground (BG) greater than 0.8. The error bars indicate the standard deviation within each group.

The temporal dynamics of VOD across different latitudes shows plausible seasonal patterns of vegetation phenology (Fig. 5). In general, summer months have the highest VOD: in the Tropics and Subtropics due to increased precipitation during that time, while in northern/southern regions due to the increased temperature and consequent vegetation growth and (leaf) biomass gain. ~~The VOD patterns strongly correlate with LAI, quantified by a Spearman coefficient of 0.67, 0.66 and 0.58 between LAI and C-, X- and Ku-band respectively~~

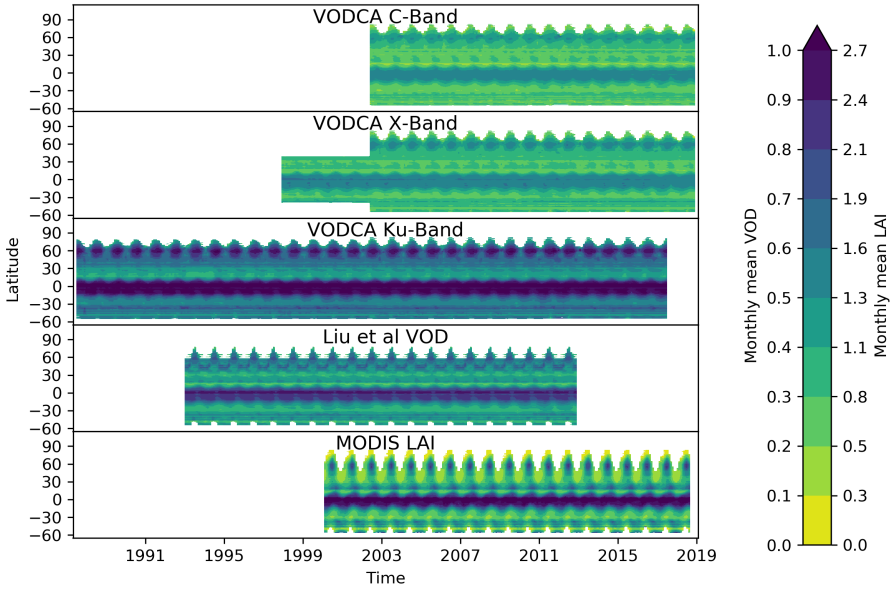

Figure 5. Hovmoeller diagrams showing the monthly mean VOD per latitude for each Band of VODCA, LiuVOD and for LAI

The VOD time series do not show any visible artificial breaks, indicating that the biases have overall been successfully removed from the individual sensors before merging. To make potential artificial breaks more visible, we investigated the seasonal anomalies per latitude (Fig. 6). The anomalies ~~, using the period from 2002 to 2017 as reference,~~ are calculated by collecting all the observations of a latitude, calculating the monthly mean, subtracting the multi-year monthly average and removing any potential linear trends using ordinary least squares regression. Hence the anomalies should either represent natural variability or artifacts due to shifts in available sensors. In the latter case, one would expect global anomalies to be visible either due to bias or differing spatial extent.

Most anomalies are limited in both space and time~~and~~ , their start or end does not coincide with a change in sensors ~~,~~ and indicating that they are due to natural causes. ~~MODIS LAI shows similar anomalies as the VOD products, the Spearman correlation coefficient is 0.29, 0.29 and 0.26 between LAI and C-, X- and Ku-band anomalies respectively.~~ Anomalies in MODIS LAI show similar patterns like VODCA anomalies, showing that surface events manifest in both in a similar way. The LiuVOD anomalies are very similar to the VODCA anomalies, the biggest difference being that the texture is less coarse due to the temporal smoothing present.

To further assess the stability of VODCA, the correlation of VOD with LAI was calculated for different blending periods similar as in Dorigo et al. (2015) (Figure 7). The blending periods are chosen for each band such that each period corresponds to a different set of input sensors (Figure 1) and that each period is long enough to calculate reliable coefficients. Both the

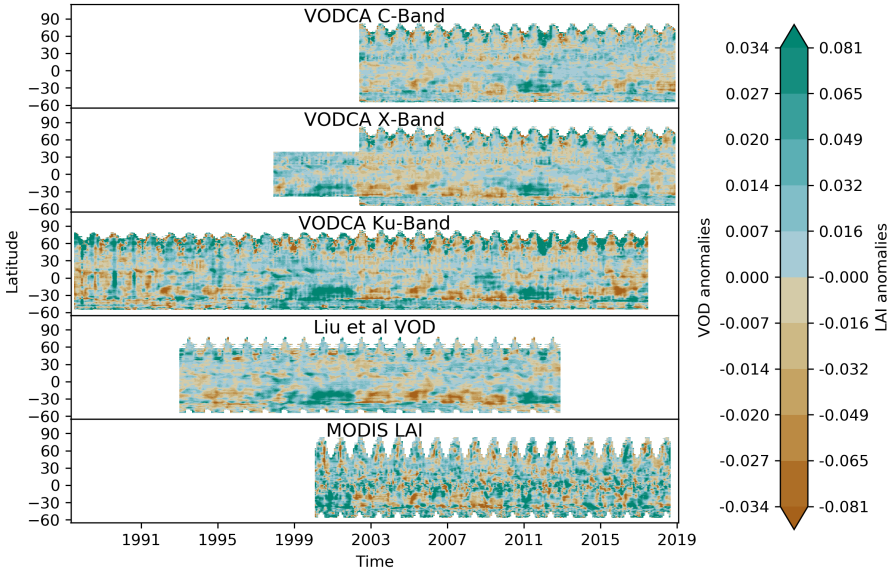

Figure 6. Hovmoeller diagrams showing anomalies of the monthly means per latitude for each band of VODCA, LiuVOD and for LAI

correlation between the raw time series as well as the anomalies indicate that the temporal dynamics are consistent over the whole length of the time series.

4.2 Spatio-temporal coverage

The temporal and spatial coverage of the merged VOD time series for each band is shown in Figure 8. The coverage of the merged products is defined by the spatial and temporal coverage of sensors (Fig. 1). For any band in any time span with at least one sensor, most parts of the globe have for at least 40% of all days an observation, while in any time period with at least two sensors about 70% of all days have a valid observation. TMI is the only sensor with a non-polar orbit of 35°N/S, leading to an increased coverage in that region in Ku- and X-band from 1997-2015. The latitude affects the coverage in multiple ways: Northern regions are generally more often covered by the polar-orbiting satellites but on the other hand, frozen grounds and snow cover inhibit the retrieval of VOD in ~~Winter~~winter. The low coverage band near 23°N is the result of LPRM not converging on a valid solution in very arid regions due to the extreme soil dielectric constants in these regions (de Jeu et al., 2014).

In some locations the merged VOD products have fewer observations than in the original products. This data loss can be caused by a failure of the merging procedure~~. The matching can fail due to~~ , in detail explained in section 3.2.4. Matching failures are always a result of insufficient AMSR-E data and hence the data loss occurs in similar regions for all sensors of one band. The lack of AMSR-E data is in most cases due to either RFI or low temperatures in mountainous regions. As an example Figure 9 shows, for all bands, where the CDF-matching failed for WindSat data. Ku-band is the least affected (Fig.

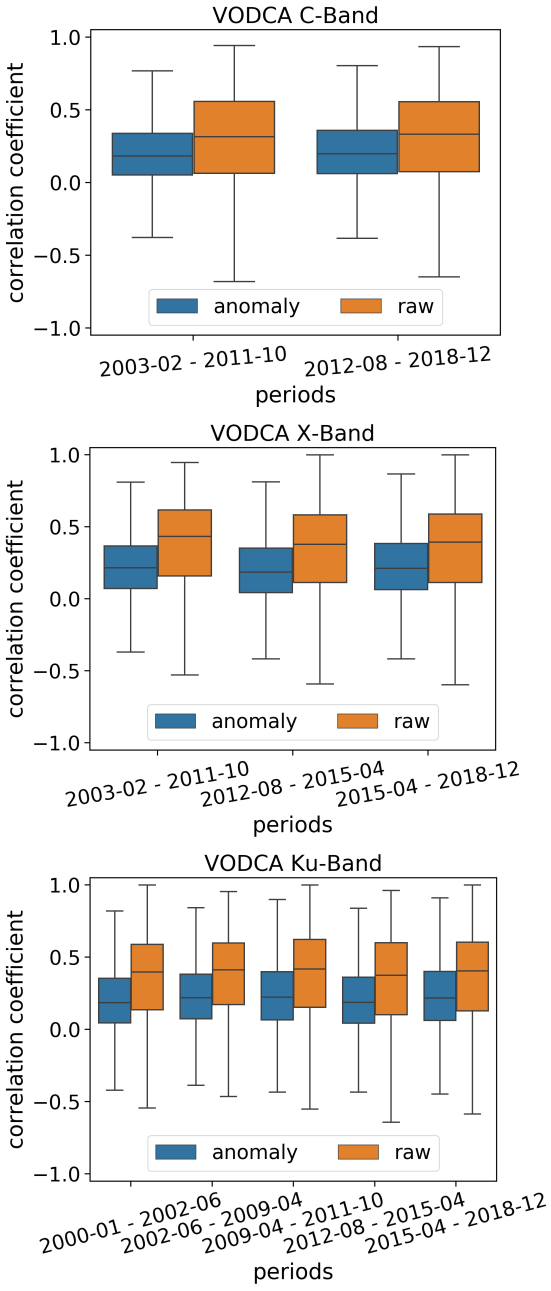

Figure 7. ~~Hovmoeller diagrams showing anomalies of the monthly means per latitude for each band of~~ Correlation between VODCA and ~~for~~ MODIS LAI, raw time series and anomalies, for different blending periods.

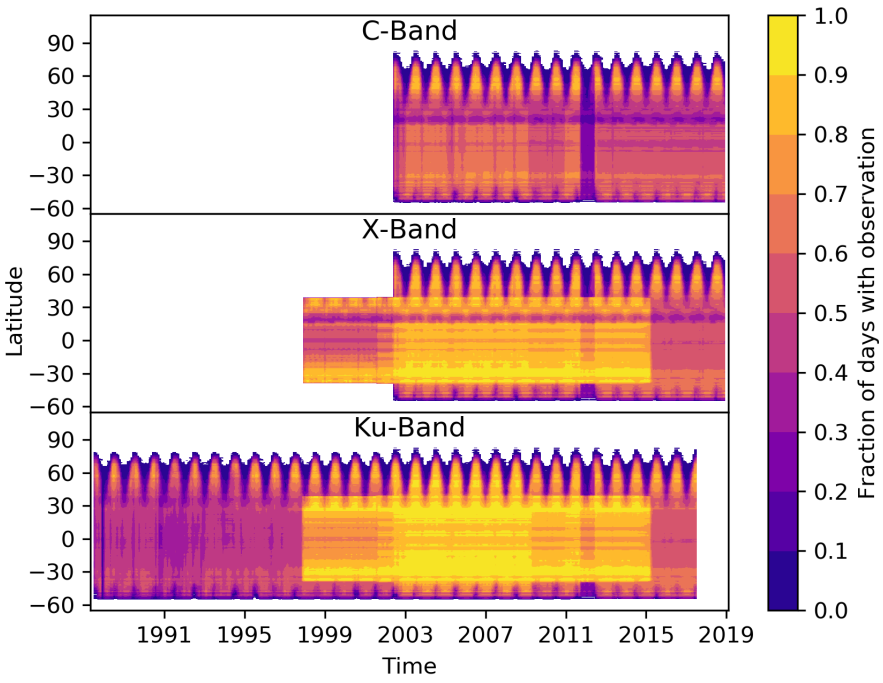

Figure 8. Hovmoeller diagrams showing for each latitude and month the fraction of ~~in~~ days ~~each month~~ per ~~latitude that have an observation~~month with observations. ~~For this figure, the~~ The number of observations ~~for each~~ of a latitude and month are counted and then divided by the number of ~~land grid points and~~ days per month and the number of land grid points at that latitude.

9 (c)), where only about 2% of the grid points are lost, mostly in the Himalayas. In X-band the matching fails for about 5% of the grid points, mostly in large parts of the Sahara (Fig. 9 (b)). C-band is most affected by data loss (10%), mostly in some parts of the USA where additional RFI prevents accurate retrievals (Fig. 9 (a)) (Njoku et al., 2005).

4.3 Random error characteristics

To validate the performance of our merging approach we evaluate the change in autocorrelation as an indicator for precision. Merging overlapping observations from multiple sensors is supposed to result in data that has a higher precision than the data of any of the individual sensors. But without a higher-quality external reference data set, assessing the change in precision is non-trivial. However, we can assume that there is supposed to be a high degree of temporal autocorrelation between subsequent observations because VOD is related to gradual changes in plant water content and biomass (Momen et al., 2017; Konings et al., 2016). Therefore we calculated the difference between the first-order temporal autocorrelation before and after merging.

The autocorrelation coefficient is strongly dependent on the temporal resolution. As seen in sec. 4.2, the temporal resolution of VODCA increases if multiple sensors are available. Therefore directly comparing the autocorrelation coefficients between the individual sensors and the merged products would lead to an increase in autocorrelation that is related to the temporal

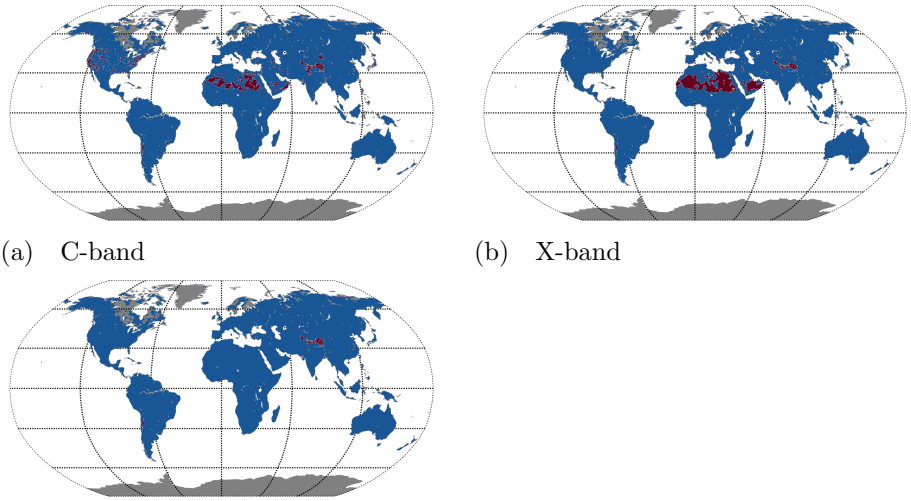

(a) C-band (b) X-band

(c) Ku-band

Figure 9. Data loss of during CDF-matching of different WindSat bands. CDF-matching failed for the red grid points and therefore the data of WindSat at that location is dropped. Very similar looking maps exist for the other sensors in the supplement Fig. 4

resolution rather than to the precision. Therefore the temporal resolution is kept unchanged by using only observation dates existing both in the pre-merge and post-merge data set.

The autocorrelation differences for X-band are shown in Figure 10. The other bands show similar results and are available in the ~~supplement Figs.~~ supplementary Figures 1-3. The autocorrelation of the merged time series is on average higher than the autocorrelation of the input series, indicating an overall decrease in noise. However, sometimes the gain in autocorrelation of one sensor mirrors the loss of the autocorrelation of the other, likely due to the former sensor being more noisy than the latter, e.g. in Alaska or east Russia in X-band of AMSR-E vs. WindSat. This means that locally, sometimes a single sensor has a higher precision than VODCA. But there are also regions where the merged VOD autocorrelation is higher than any of the input time series, e.g in Europe or central north America. This is likely to occur when all sensors have a similar precision, meaning that none of them is dragging the precision of the others down.

A noteworthy case is TMI where the autocorrelation of the merged time series is almost always higher. This could mean that the TMI data is very noisy and is dragging the overall quality of the merged data down. We investigated this possibility by experimentally not including TMI in VODCA. This resulted in average in a lower gain in autocorrelation for the other data sets, indicating that the TMI data is still positively ~~contribute~~ contributing to the precision of the merged products by reducing the noise of the end product~~(result not shown)~~.

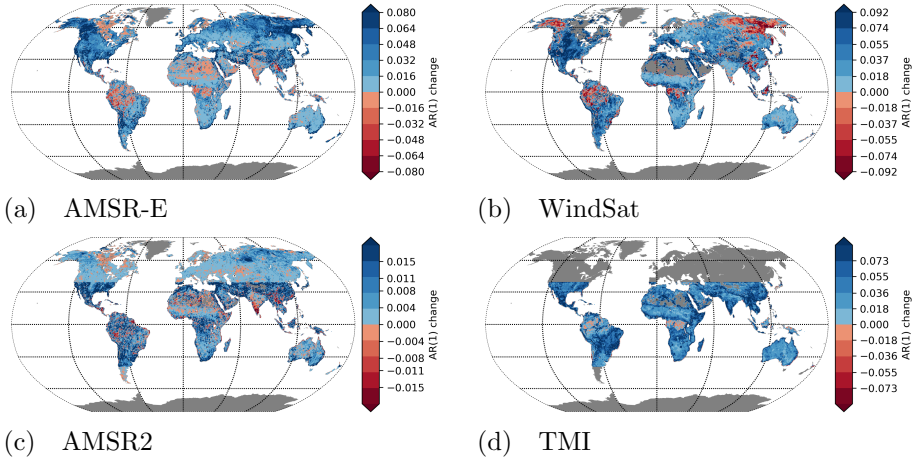

Figure 10. First-order auto-correlation change due to merging of X-band data for each sensor.

4.4 Comparison of ~~VOD~~ VODCA with LAI, LiuVOD and Vegetation Continuous Fields

4.4.1 ~~Correlation between VOD and LAI~~

4.4.1 Correlation between VOD and LAI

A direct validation of VODCA is not possible because of the lack of appropriate in situ measurements. Hence it is only possible to assess dynamics in VOD with dynamics in related variables such as LAI or land cover. Globally, LAI and ~~VOD~~ VODCA time series and their seasonal anomalies are positively correlated over large areas (~~Fig.~~ Figure 11). For all bands, the highest correlations with LAI can be found in grassland-dominated regions such as in African Savannahs, Australia and in parts of South America. Correlations are usually lower in forested regions and even slightly negative in parts of tropical forests such as in the Amazon. The negative correlations in tropical forests could be caused by drought periods where vegetation water content and hence VOD should decline but LAI possibly increases (Myneni et al., 2007; Saleska et al., 2007), although a green-up of the Amazon under drought is highly debated (Samanta et al., 2010, 2012; Morton et al., 2014). However, this comparison of ~~VOD~~ VODCA and LAI demonstrates that ~~the merged VOD products reflect~~ VODCA reflects plausible seasonal and short-term changes in vegetation and will likely provide additional information on vegetation dynamics on top of LAI and other related optical biophysical vegetation products from optical remote sensing.

To assess differences between the temporal dynamics of VODCA and LiuVOD, we compared both to MODIS LAI. Because LiuVOD is temporally smoothed, comparing daily values is inadequate. Instead, we first resample both datasets to monthly averages and calculate the Spearman correlation to the also monthly averaged MODIS LAI, only using dates existing in all datasets. The downsampling leads to slightly higher correlation coefficients (Figure 12) than using the daily values (Figure 11) due to decreased noise, while the spatial patterns stay the same. The highest correlation has VODCA X-band, with a global

average of 0.42, followed by VODCA Ku- and C-band with 0.39 and 0.37 respectively. Lowest in average is LiuVOD with 0.33. It could be that the lower correlation is a result of being a mix of multiple bands or because the VODCA products use more input datasets, resulting in more accurate values. Either way, this indicates that the VODCA products capture temporal dynamics better.

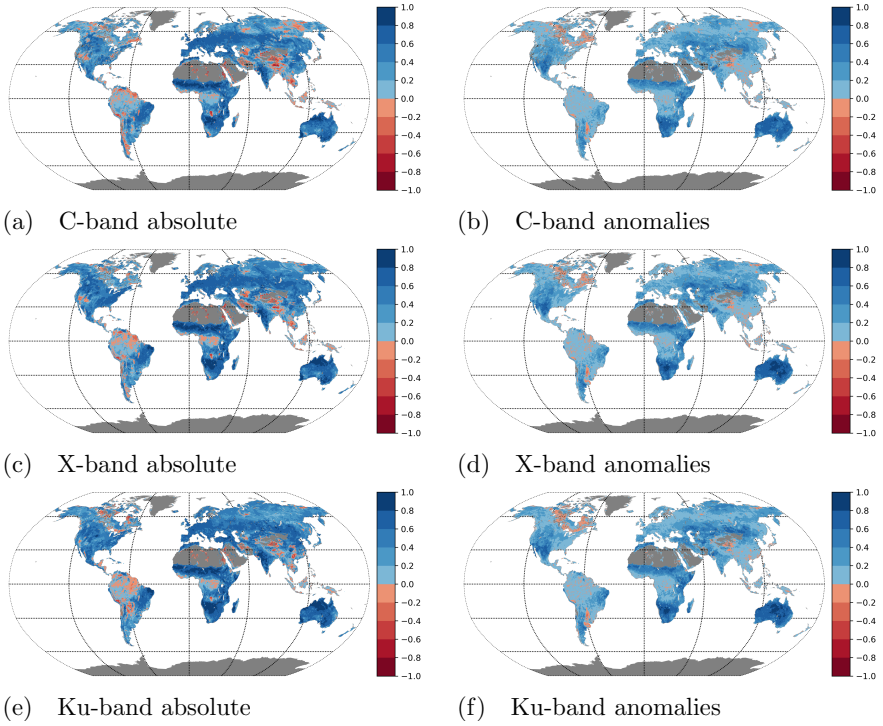

Figure 11. Spearman correlation coefficient between VODCA VOD and MODIS LAI for each band. The left column shows the correlation for the absolute signal, the right column for the anomalies from the long-term VOD climatology.

4.4.2 ~~Trend—analysis of VOD, LAI and Vegetation Continuous Fields~~

4.4.2 Trend-analysis of VODCA, LiuVOD, LAI and Vegetation Continuous Fields

To evaluate the relationship between C-, X-, Ku-band ~~VOD~~VODCA, LiuVOD, MODIS LAI and VCF changes and to gain a first insight into the long-term changes in VOD we assess linear trends in the data sets. Yearly averages are used to determine the trends and their confidence intervals via the Theil–Sen estimator. Trends whose upper and lower confidence interval do not have the same sign or either of them is zero are regarded as non-significant and are not displayed ~~. Fig. 11~~ in Figures 13, 15 and 14 . Figures 13 (a-c) show the C-, X- and Ku-band VODCA trends from 2002-06-19 to 2017-06-19 during which all bands have global coverage. The trends are visually very similar in all bands, confirmed by the spatial Spearman correlation coefficients

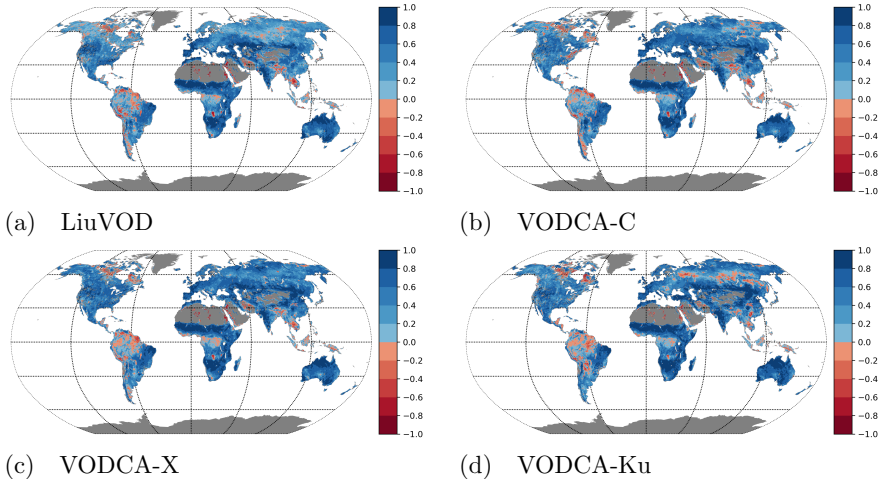

(a) LiuVOD (b) VODCA-C

(c) VODCA-X (d) VODCA-Ku

Figure 12. ~~Spearman correlation coefficient between merged VOD~~ Correlation of monthly LiuVOD and the VODCA products with MODIS LAI~~for each band~~. ~~In~~ For this analysis, the ~~left column~~ data are ~~the coefficients between the raw values~~first resampled to monthly averages, ~~in the right between~~ then only the ~~anomalies~~months where all four data sets have values are used.

of 0.88 between the C- and X-band trends, 0.89 between C- and Ku-band and 0.91 between X- and Ku-band, calculated using only locations where both bands have a significant trend. This further reinforces that all bands react very similarly to vegetation changes. The spatial overlap of trends is shown in ~~Fig. 11~~ Figure 13 (d), where each location is classified based on the sum of positive and the sum of negative trends. Locations with no significant trend in any band are not displayed. The three classes with contradicting trends (1|1, 2|1, 1|2) are rare as together they make up only 4.2% of the displayed points. Conversely, 48% of the land points are covered by the four classes with at least two agreeing trend directions without any contradicting trend (2|0, 3|0, 0|2, 0|3). The agreement in trends between frequencies indicates that the longer Ku-band series can be used as indicator of the shorter X- and C-band series in trend analyses. Further, the LAI trends of the same time period (Fig. ~~??~~ 13 (e)) match the VOD trends very well overall, even though in detail the strength and location of the trends vary.

The trends of Ku-band VODCA and LiuVOD were determined (Figure 14) to asses whether studies that have been analyzing VOD trends using LiuVOD would get different results if they were repeated using VODCA Ku-band instead. Ku-band VODCA is used because it has the longest overlap with LiuVOD (1993 to 2012).

On a global scale, we see the almost exact same patterns in both VOD series, therefore studies performed at that scale would get similar results for both data sets. However, on a local scale the patterns differ simethimes; E.g. in most of Turkey Ku-band VODCA shows an increase, while LiuVOD shows a decrease in VOD. As such regional studies might get case-by-case very different results depending on which dataset is used.

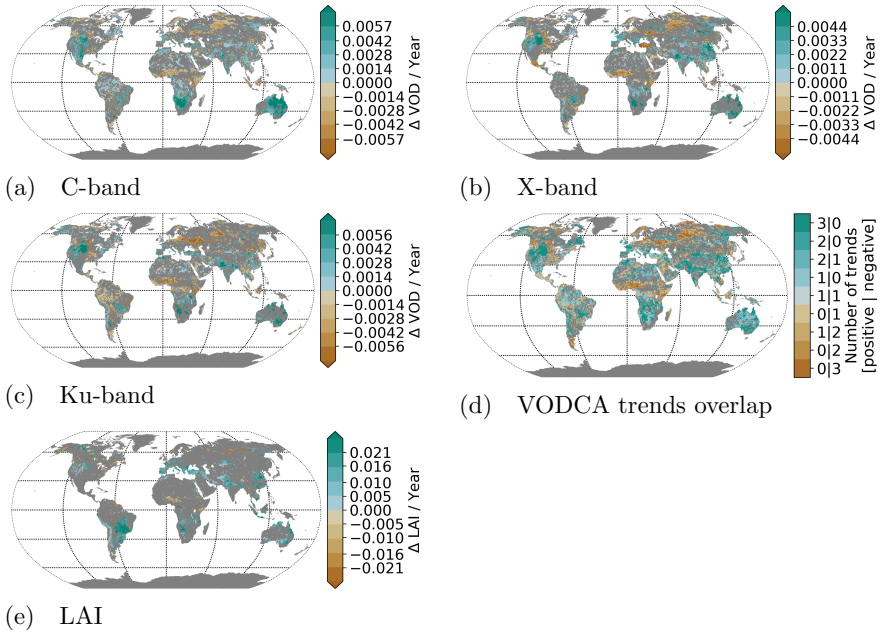

Figure 13. Trends of various bands between 2002 to 2017 of VOD (a-c) and LAI (e). Non-significant trends are not displayed, the trends are calculated by Theil-Sen regression using yearly mean values. Figure (d) shows trend classes based on the number of VOD bands showing a positive|negative trend. Their order and color are indicative of the likelihood of the trend.

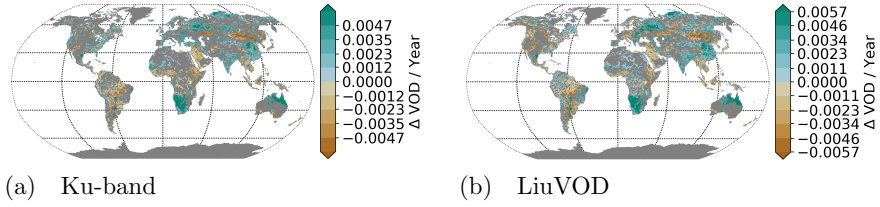

Figure 14. Trends between 1993 to 2012 of Ku-band VODCA (a) and LiuVOD (b). Non-significant trends are not displayed, the trends are calculated by Theil-Sen regression using yearly mean values.

Taking advantage of the much longer length of the Ku-band, another trend analysis is done for this band using the data from 1987 - ~~2017~~ 2016 (Fig. ~~??~~ 15 (g)) to give a first impression of the changes within the last thirty years. Overall we see a decline in VOD in the tropics, likely due to deforestation, and in large parts of Mongolia, attributed to variations in rainfall and surface temperatures as well as increased life stock farming and wild fires (Liu et al., 2013). VOD increased strongly in India and large parts of China, mostly due to an increase in croplands in the former case and due to both an increase in forest

and croplands in the latter (Chen et al., 2019). VOD also increased in northern parts of Australia, matching trends in FPAR and precipitation seen in Donohue et al. (2009). Other regions with increasing VOD are south Africa and central north America. Of a questionable nature is the wide spread positive trend in the Sahara given LPRMs struggle to retrieve VOD here. Most of the changes observed for VOD are mirrored in the VCF changes from 1987 to 2016 (Fig. ~~??~~ 15 (f), see sec. 2.2.3 for details). The large bare ground losses in India, China and the north African shrubland manifest as positive VOD trends. Likewise, the deforestation in south America and land degradation with hotspots in Mongolia, Afghanistan or southwestern USA coincide with a loss in VOD. Also the patterns of tree cover gain in eastern Europe and European Russia coincide with increased VOD. While there do not seem to be any areas where VOD and VCF contradict each other clearly, some trends are only visible in one of the data sets. For example the strong increase in VOD in southern Africa cannot be observed in VCF.

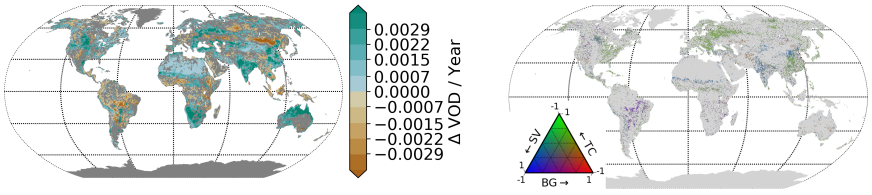

(a) Ku-band (b) Land cover changes

Figure 15. ~~Trend analyses for various bands and time spans~~ Trends between 1987 to 2016 of Ku-band VOD (~~a-c, f), LAI (~~ea) and tree canopy, short vegetation and bare ground (~~g~~b). Non-significant trends are not displayed, the trends are calculated by ~~linear regression~~ Theil-Sen estimator using yearly mean values. ~~Figure (d) shows trend classes based on the number of VOD bands showing a positive|negative trend. Their order and color are indicative of the likelihood of the trend.~~

5 Current limitations and possible improvements

5.1 AMSR2 scaling to TMI

Upon closer inspection of the trends in Figure ~~??~~13, we can see in north America a spatial break in X- and Ku-band trends at 35°N. North of this latitude AMSR2 data of 2012-2014 ~~have been~~ were matched to the AMSR-E data of 2010-2012~~north of this latitude and in the south to temporally overlapping observations of scaled TMI~~ , while south of this line temporally overlapping scaled TMI values were used to bridge the gap between the two sensors. Unusual low VOD values can be observed in ~~time series of that~~ this region in the years 2012 to 2015 in both X-and Ku-band. This indicates that the CDF-matching does not correct the bias between the sensors but artificially removes the difference that ~~are~~ is due to surface processes. Consequently, the matched AMSR2 data has a slight positive bias north of 35°N in large parts of north America. For users we advise to be careful when using X- and Ku-band ~~observations~~ values after July 2012 north/south of 35°N/S as well as C-band ~~observations~~ values after July 2012 globally as the AMSR2 data might induce a bias. Currently there exists a flag indicating how AMSR2

has been CDF-matched. With ongoing AMSR-E vs. AMSR2 Level 1 intercalibration efforts by JAXA we expect to reduce spurious observations in the AMSR2 period in th enear future.

5.2 Data loss while CDF-matching

As described earlier, ~~CDF matching~~ CDF-matching failed because of missing AMSR-E data in some regions, mostly in the Himalayas (Fig. 9). One possible solution to avoid this data loss would be to substitute the CDF-matching parameters of these locations with the parameters from locations with similar dynamics in VOD. This could be done by clustering the time series and using the parameters of another location within the same cluster. Taking this one step further, one could also investigate the possibility of using all the data in one cluster to derive a single set of CDF-matching parameters and use these to scale all the source time series within it. Not only would this allow to scale all the data without loss, but the increased number of ~~observations~~ values available for each parameter determination would also lead to more robust CDF-parameters. However, generating meaningful clusters from hundreds of thousands long time series containing missing ~~observations~~ values while keeping the computational cost at bay is anything but trivial (e.g. Mikalsen et al. (2018)). Besides, even though clusters may be composed of time series with very similar characteristics, the VOD signal at each location may still have its unique features resulting e.g., from land surface characteristics or vegetation species composition.

5.3 Data gaps in the input data sets leading to increased noise

Averaging multiple temporally overlapping observations reduces noise (sec. 4.3). However, this can be only done if overlapping observations exist. While theoretically the maximum number of observations is ~~limited to~~ defined by the number of available sensors, ~~usually less~~ in practise usually fewer observations are available due to gaps in the individual time series~~of each sensor. Hencea potential short-time gap-filling of~~ . Hence, filling short gaps in the original time series of each sensor could potentially increase the precision of VODCA. Since VOD changes slowly over time (Konings et al., 2016), it is intuitively clear that even if a sensor has no valid observation on a certain date, the value is expected to be similar to the value of the dates before and after. Therefore one could fill short gaps with a model that at least ~~implicit~~ implicitly uses autocorrelation for its predictions, such as gaussian processes ~~as in Camps-valls et al. (2017).~~ (Camps-valls et al., 2017).

5.4 L-band product

An L-band product would be of great use to the scientific community, as L-band VOD has been instrumental in analyzing vegetation patterns (e.g. Brandt et al. (2018a); Tian et al. (2018); Brandt et al. (2018b); Chaparro et al. (2018)). Although we produced an experimental L-band product based on LPRM-SMAP and LPRM-SMOS using the same methodologies as for the other bands, the evaluation of this L-band product showed that it is not yet fit for release for a number of reasons. First, merging SMOS and SMAP does not result in a time series that is longer than just SMOS alone, therefore in terms of temporal extent nothing is gained. Second, the temporal coverage is highly unbalanced, with the SMAP period having a much higher density.

This carries the high risk that users might apply unfitting methods to the data. Third, the autocorrelation analysis indicated that VODCA-L has a higher level of noise than pure LPRM-SMAP. Nevertheless, given the great scientific interest in L-band VOD, we continue working on a VODCA L-band product. Yet, a lot of work is still required, such as assessing the impact of the VOD retrieval algorithms (e.g., LPRM SMAP and SMOS (van der Schalie et al., 2017; Owe et al., 2008; Meesters et al., 2005) , SMOS-IC (Fernandez-Moran et al., 2017) and MT-DCA (Konings et al., 2016)), and developing more suitable merging algorithms that can deal with the low temporal variability of L-band VOD compared to the other frequencies.

5.5 Effect of merging different observation times and geometries

Litarature has shown that the observation time has an influence on the retrieved VOD (Konings and Gentine, 2017; Konings et al., 2017) and that the spatial footprint and resampling method and the resmpling reference time affect the quality of merged soil moisture products (Dorigo et al., 2015). However, overall very little knowledge currently exists about the effect of mixing observation times and sensor geometries (incidence angles, spatial footprint,...) of multiple VOD values. Further research on these topics would improve the understanding of VOD and may lead to more advanced merging procedures that take these effects into account.

6 Conclusions

~~We present to the scientific community~~ In this paper we presented VODCA, three ~~long term~~ long-term VOD data sets spanning ~~the last three decades to~~ up to three decades that can be used in studies of the biosphere. ~~For the most part we~~ We were able to remove most of the biases between the different input sensors by co-calibrating them to AMSR-E. The merging leads to observations with less noise than the input data sets. The trends of the different ~~VOD bands~~ VODCA products (C-, X-, Ku-band) correlate very strongly with each other and show similar spatial distributions and temporal dynamics as trends in LAI and VCF~~, with the added benefit of having observations on a daily basis~~ . Compared to the latter products, which are based on solar-reflective remote sensing, VOD has the benefit of being unaffected by cloud cover, allowing generally for more than 40% of days having a valid VOD observation. A major ongoing issue is the potential bias in AMSR2 due to no temporally overlapping observations with other sensors. ~~This and other problems still have to be resolved and as such we plan to maintain and improve VODCA with up-to-date data and continued development for the foreseeable future~~Future efforts will focus on resolving this and other issues while future VODCA releases will continuously update the climate archive with recent observations.

Data availability. The VODCA products (Moesinger et al., 2019) are open access (Attribution 4.0 International) and available at Zenodo https://doi.org/10.5281/zenodo.2575599

Author contributions. Wouter Dorigo, Leander Moesinger, and Matthias Forkel designed the study. Leander Moesinger performed the analyses and wrote the manuscript together with Matthias Forkel and Wouter Dorigo. All authors contributed to discussions about the methods and results and provided feedback on the manuscript.

Competing interests. The authors declare that they have no conflict of interest

Acknowledgements. The MODIS LAI data (MOD15A2H, v006) by Myneni et al. (2015) were retrieved from the online data pool, courtesy of the NASA EOSDIS Land Processes Distributed Active Archive Center (LP DAAC), USGS/Earth Resources Observation and Science (EROS) Center, Sioux Falls, South Dakota, https://lpdaac.usgs.gov/data_access/data_pool .

The VCF annual data (VCF5KYR, v001) by Hansen and Song (2018) were retrieved from the online NASA Earthdata Search, courtesy of the NASA EOSDIS Land Processes Distributed Active Archive Center (LP DAAC), USGS/Earth Resources Observation and Science (EROS) Center, Sioux Falls, South Dakota, https://search.earthdata.nasa.gov .

The authors acknowledge the TU Wien University Library for financial support through its Open Access Funding Program.

References

Brandt, M., Wigneron, J.-P., Chave, J., Tagesson, T., Penuelas, J., Ciais, P., Rasmussen, K., Tian, F., Mbow, C., Al-Yaari, A., Rodriguez-Fernandez, N., Schurgers, G., Zhang, W., Chang, J., Kerr, Y., Verger, A., Tucker, C., Mialon, A., Rasmussen, L. V., Fan, L., and Fensholt, R.: Satellite passive microwaves reveal recent climate-induced carbon losses in African drylands, Nature Ecology & Evolution, 2, 827–835, https://doi.org/10.1038/s41559-018-0530-6, http://www.nature.com/articles/s41559-018-0530-6, 2018a.

Brandt, M., Yue, Y., Wigneron, J. P., Tong, X., Tian, F., Jepsen, M. R., Xiao, X., Verger, A., Mialon, A., Al-Yaari, A., Wang, K., and Fensholt, R.: Satellite-observed Major Greening and Biomass Increase in South China Karst During Recent Decade, Earth's Future, https://doi.org/10.1029/2018EF000890, http://doi.wiley.com/10.1029/2018EF000890, 2018b.

Camps-valls, G., Svendsen, D. H., Martino, L., and Campos-t, M.: Physics-Aware Gaussian Processes for Earth Observation, 10270, https://doi.org/10.1007/978-3-319-59129-2, http://link.springer.com/10.1007/978-3-319-59129-2, 2017.

Chaparro, D., Piles, M., Vall-llossera, M., Camps, A., Konings, A. G., and Entekhabi, D.: L-band vegetation optical depth seasonal metrics for crop yield assessment, Remote Sensing of Environment, 212, 249–259, https://doi.org/10.1016/J.RSE.2018.04.049, https://www.sciencedirect.com/science/article/pii/S0034425718302062{#}bb0240, 2018.

Chen, C., Park, T., Wang, X., Piao, S., Xu, B., Chaturvedi, R. K., Fuchs, R., Brovkin, V., Ciais, P., Fensholt, R., Tømmervik, H., Bala, G., Zhu, Z., Nemani, R. R., and Myneni, R. B.: China and India lead in greening of the world through land-use management, Nature Sustainability, 2, 122–129, https://doi.org/10.1038/s41893-019-0220-7, http://www.nature.com/articles/s41893-019-0220-7, 2019.

de Jeu, R. A., Holmes, T. R., Parinussa, R. M., and Owe, M.: A spatially coherent global soil moisture product with improved temporal resolution, Journal of Hydrology, 516, 284–296, https://doi.org/10.1016/J.JHYDROL.2014.02.015, https://www.sciencedirect.com/science/article/pii/S0022169414001139, 2014.

de Nijs, A. H. A., Parinussa, R. M., de Jeu, R. A. M., Schellekens, J., and Holmes, T. R. H.: A Methodology to Determine Radio-Frequency Interference in AMSR2 Observations, IEEE Transactions on Geoscience and Remote Sensing, 53, 5148–5159, https://doi.org/10.1109/TGRS.2015.2417653, http://ieeexplore.ieee.org/document/7116527/, 2015.

Donohue, R. J., Mcvicar, T. R., and Roderick, M. L.: Climate-related trends in Australian vegetation cover as inferred from satellite observations, 1981-2006, Global Change Biology, 15, 1025–1039, https://doi.org/10.1111/j.1365-2486.2008.01746.x, http://doi.wiley.com/10.1111/j.1365-2486.2008.01746.x, 2009.

Dorigo, W., De Jeu, R., Chung, D., Parinussa, R., Liu, Y., Wagner, W., and Fernández-Prieto, D.: Evaluating global trends (1988-2010) in harmonized multi-satellite surface soil moisture, Geophysical Research Letters, 39, 3–9, https://doi.org/10.1029/2012GL052988, 2012.

Dorigo, W., Gruber, A., De Jeu, R., Wagner, W., Stacke, T., Loew, A., Albergel, C., Brocca, L., Chung, D., Parinussa, R., and Kidd, R.: Evaluation of the ESA CCI soil moisture product using ground-based observations, Remote Sensing of Environment, 162, 380–395, https://doi.org/10.1016/J.RSE.2014.07.023, https://www.sciencedirect.com/science/article/pii/S0034425714002727?via{%}3Dihub{#}f0045, 2015.

Dorigo, W., Wagner, W., Albergel, C., Albrecht, F., Balsamo, G., Brocca, L., Chung, D., Ertl, M., Forkel, M., Gruber, A., Haas, E., Hamer, P. D., Hirschi, M., Ikonen, J., de Jeu, R., Kidd, R., Lahoz, W., Liu, Y. Y., Miralles, D., Mistelbauer, T., Nicolai-Shaw, N., Parinussa, R., Pratola, C., Reimer, C., van der Schalie, R., Seneviratne, S. I., Smolander, T., and Lecomte, P.: ESA CCI Soil Moisture for improved Earth system understanding: State-of-the art and future directions, Remote Sensing of Environment, 203, 185–215, https://doi.org/10.1016/j.rse.2017.07.001, http://linkinghub.elsevier.com/retrieve/pii/S0034425717303061, 2017.

Fan, L., Wigneron, J.-P., Xiao, Q., Al-Yaari, A., Wen, J., Martin-StPaul, N., Dupuy, J.-L., Pimont, F., Al Bitar, A., Fernandez-Moran, R., and Kerr, Y.: Evaluation of microwave remote sensing for monitoring live fuel moisture content in the Mediterranean region, Remote Sensing of Environment, 205, 210–223, https://doi.org/10.1016/J.RSE.2017.11.020, https://www.sciencedirect.com/science/article/pii/S0034425717305692, 2018.

Fernandez-Moran, R., Al-Yaari, A., Mialon, A., Mahmoodi, A., Al Bitar, A., De Lannoy, G., Rodriguez-Fernandez, N., Lopez-Baeza, E., Kerr, Y., and Wigneron, J.-P.: SMOS-IC: An Alternative SMOS Soil Moisture and Vegetation Optical Depth Product, Remote Sensing, 9, 457, https://doi.org/10.3390/rs9050457, http://www.mdpi.com/2072-4292/9/5/457, 2017.

Forkel, M., Dorigo, W., Lasslop, G., Teubner, I., Chuvieco, E., and Thonicke, K.: A data-driven approach to identify controls on global fire activity from satellite and climate observations (SOFIA V1), Geoscientific Model Development, 10, 4443–4476, https://doi.org/10.5194/gmd-10-4443-2017, https://www.geosci-model-dev.net/10/4443/2017/, 2017.

Forkel, M., Dorigo, W., Lasslop, G., Chuvieco, E., Hantson, S., Heil, A., Teubner, I., Thonicke, K., and Harrison, S. P.: Recent global and regional trends in burned area and their compensating environmental controls, Environmental Research Communications, 1, 051 005, https://doi.org/10.1088/2515-7620/ab25d2, https://doi.org/10.1088%2F2515-7620%2Fab25d2, 2019.

Gaiser, P. W., St. Germain, K. M., Twarog, E. M., Poe, G. A., Purdy, W., Richardson, D., Grossman, W., Jones, W. L., Spencer, D., Golba, G., Cleveland, J., Choy, L., Bevilacqua, R. M., and Chang, P. S.: The windSat spaceborne polarimetric microwave radiometer: Sensor description and early orbit performance, IEEE Transactions on Geoscience and Remote Sensing, 42, 2347–2361, https://doi.org/10.1109/TGRS.2004.836867, 2004.

Giardina, F., Konings, A. G., Kennedy, D., Alemohammad, S. H., Oliveira, R. S., Uriarte, M., and Gentine, P.: Tall Amazonian forests are less sensitive to precipitation variability, Nature Geoscience, 11, 405–409, https://doi.org/10.1038/s41561-018-0133-5, http://www.nature.com/articles/s41561-018-0133-5, 2018.

Grant, J. P., Wigneron, J.-P., De Jeu, R. A. M., Lawrence, H., Mialon, A., Richaume, P., Al Bitar, A., Drusch, M., Van Marle, M. J. E., and Kerr, Y.: Comparison of SMOS and AMSR-E vegetation optical depth to four MODIS-based vegetation indices, Remote Sensing of Environment, 172, 87–100, https://doi.org/10.1016/j.rse.2015.10.021, https://ac.els-cdn.com/S0034425715301735/1-s2.0-S0034425715301735-main.pdf?{_}tid=fd05dbf8-2a49-438c-8f7f-dce794bb90a6{&}acdnat=1524568420{_}3f2adbe057045116fcd23d7de2f827ab, 2016.

Green, S. B.: How Many Subjects Does It Take To Do A Regression Analysis, Multivariate Behavioral Research, 26, 499–510, https://doi.org/10.1207/s15327906mbr2603_7, http://www.tandfonline.com/doi/abs/10.1207/s15327906mbr2603{_}7, 1991.

Gruber, A., Dorigo, W. A., Crow, W., and Wagner, W.: Triple Collocation-Based Merging of Satellite Soil Moisture Retrievals, IEEE Transactions on Geoscience and Remote Sensing, 55, 6780–6792, https://doi.org/10.1109/TGRS.2017.2734070, 2017.

Gruber, A., Scanlon, T., Van der Schalie, R., Wagner, W., and Dorigo, W. A.: Evolution of the ESA CCI Soil Moisture Climate Data Records and their underlying merging methodology (Manuscript in Preparation), 2019.

Hansen, M. and Song, X.: Vegetation Continuous Fields (VCF) Yearly Global 0.05 Deg [Data set], https://doi.org/10.5067/MEaSUREs/VCF/VCF5KYR.001, 2018.

Holmes, T. R. H., De Jeu, R. A. M., Owe, M., and Dolman, A. J.: Land surface temperature from Ka band (37 GHz) passive microwave observations, Journal of Geophysical Research, 114, D04 113, https://doi.org/10.1029/2008JD010257, http://doi.wiley.com/10.1029/2008JD010257, 2009.

Jackson, T. and Schmugge, T.: Vegetation effects on the microwave emission of soils, Remote Sensing of Environment, 36, 203–212, https://doi.org/10.1016/0034-4257(91)90057-D, https://www.sciencedirect.com/science/article/pii/003442579190057D, 1991.

Jones, M. O., Jones, L. A., Kimball, J. S., and McDonald, K. C.: Satellite passive microwave remote sensing for monitoring global land surface phenology, Remote Sensing of Environment, 115, 1102–1114, https://doi.org/10.1016/J.RSE.2010.12.015, https://www.sciencedirect.com/science/article/pii/S0034425710003615, 2011.

Kawanishi, T., Sezai, T., Ito, Y., Imaoka, K., Takeshima, T., Ishido, Y., Shibata, A., Miura, M., Inahata, H., and Spencer, R.: The advanced microwave scanning radiometer for the earth observing system (AMSR-E), NASDA's contribution to the EOS for global energy and water cycle studies, IEEE Transactions on Geoscience and Remote Sensing, 41, 184–194, https://doi.org/10.1109/TGRS.2002.808331, http://ieeexplore.ieee.org/document/1196037/, 2003.

Kerr, Y. H., Wigneron, J.-P., Al Bitar, A., Al-Yaari, A., Kaminski, T., Richaume, P., Mermoz, S., Rodríguez-Fernández, N. J., Mialon, A., Le Toan, T., Bouvet, A., and Brandt, M.: An evaluation of SMOS L-band vegetation optical depth (L-VOD) data sets: high sensitivity of L-VOD to above-ground biomass in Africa, Biogeosciences, 15, 4627–4645, https://doi.org/10.5194/bg-15-4627-2018, 2018.

Knowles, K., Savoie, M., Armstrong, R., and Brodzik, M. J.: AMSR-E/Aqua Daily EASE-Grid Brightness Temperatures, https://doi.org/https://doi.org/10.5067/XIMNXRTQVMOX, 2006.

Konings, A. G. and Gentine, P.: Global variations in ecosystem-scale isohydricity, Global Change Biology, 23, 891–905, https://doi.org/10.1111/gcb.13389, http://doi.wiley.com/10.1111/gcb.13389, 2017.

Konings, A. G., Piles, M., Rötzer, K., McColl, K. A., Chan, S. K., and Entekhabi, D.: Vegetation optical depth and scattering albedo retrieval using time series of dual-polarized L-band radiometer observations, Remote Sensing of Environment, 172, 178–189, https://doi.org/10.1016/J.RSE.2015.11.009, https://www.sciencedirect.com/science/article/pii/S003442571530198X, 2016.

Konings, A. G., Yu, Y., Xu, L., Yang, Y., Schimel, D. S., and Saatchi, S. S.: Active microwave observations of diurnal and seasonal variations of canopy water content across the humid African tropical forests, Geophysical Research Letters, 44, 2290–2299, https://doi.org/10.1002/2016GL072388, https://onlinelibrary.wiley.com/doi/abs/10.1002/2016GL072388, 2017.

Konings, A. G., Rao, K., and Steele-Dunne, S. C.: Macro to micro: microwave remote sensing of plant water content for physiology and ecology, New Phytologist, 223, nph.15 808, https://doi.org/10.1111/nph.15808, https://onlinelibrary.wiley.com/doi/abs/10.1111/nph.15808, 2019.

Kummerow, C., Barnes, W., Kozu, T., Shiue, J., Simpson, J., Kummerow, C., Barnes, W., Kozu, T., Shiue, J., and Simpson, J.: The Tropical Rainfall Measuring Mission (TRMM) Sensor Package, Journal of Atmospheric and Oceanic Technology, 15, 809–817, https://doi.org/10.1175/1520-0426(1998)015<0809:TTRMMT>2.0.CO;2, http://journals.ametsoc.org/doi/abs/10.1175/1520-0426{%}281998{%}29015{%}3C0809{%}3ATTRMMT{%}3E2.0.CO{%}3B2, 1998.

Lefsky, M. A., Harding, D. J., Keller, M., Cohen, W. B., Carabajal, C. C., Del Bom Espirito-Santo, F., Hunter, M. O., and de Oliveira, R.: Estimates of forest canopy height and aboveground biomass using ICESat, Geophysical Research Letters, 32, n/a–n/a, https://doi.org/10.1029/2005GL023971, http://doi.wiley.com/10.1029/2005GL023971, 2005.

Liu, H., Zhan, Q., Yang, C., and Wang, J.: Characterizing the Spatio-Temporal Pattern of Land Surface Temperature through Time Series Clustering: Based on the Latent Pattern and Morphology, Remote Sensing, 10, 654, https://doi.org/10.3390/rs10040654, http://www.mdpi.com/2072-4292/10/4/654, 2018.

Liu, Y., Dorigo, W., Parinussa, R., de Jeu, R., Wagner, W., McCabe, M., Evans, J., and van Dijk, A.: Trend-preserving blending of passive and active microwave soil moisture retrievals, Remote Sensing of Environment, 123, 280–297, https://doi.org/10.1016/J.RSE.2012.03.014, https://www.sciencedirect.com/science/article/pii/S0034425712001332, 2012.

Liu, Y. Y., van Dijk, A. I. J. M., de Jeu, R. A. M., and Holmes, T. R. H.: An analysis of spatiotemporal variations of soil and vegetation moisture from a 29-year satellite-derived data set over mainland Australia, Water Resources Research, 45, https://doi.org/10.1029/2008WR007187, http://doi.wiley.com/10.1029/2008WR007187, 2009.

Liu, Y. Y., De Jeu, R. A. M., McCabe, M. F., Evans, J. P., and Van Dijk, A. I. J. M.: Global long-term passive microwave satellite-based retrievals of vegetation optical depth, Geophysical Research Letters, 38, 1–6, https://doi.org/10.1029/2011GL048684, 2011a.

Liu, Y. Y., de Jeu, R. A. M., McCabe, M. F., Evans, J. P., and van Dijk, A. I. J. M.: Global long-term passive microwave satellite-based retrievals of vegetation optical depth, Geophysical Research Letters, 38, n/a–n/a, https://doi.org/10.1029/2011GL048684, http://doi.wiley.com/10.1029/2011GL048684, 2011b.

Liu, Y. Y., Parinussa, R. M., Dorigo, W. A., De Jeu, R. A. M., Wagner, W., Van Dijk, A. I. J. M., Mccabe, M. F., and Evans, J. P.: Developing an improved soil moisture dataset by blending passive and active microwave satellite-based retrievals, Hydrol. Earth Syst. Sci, 15, 425–436, https://doi.org/10.5194/hess-15-425-2011, www.hydrol-earth-syst-sci.net/15/425/2011/, 2011c.

Liu, Y. Y., Evans, J. P., McCabe, M. F., de Jeu, R. A. M., van Dijk, A. I. J. M., Dolman, A. J., and Saizen, I.: Changing Climate and Overgrazing Are Decimating Mongolian Steppes, PLoS ONE, 8, e57 599, https://doi.org/10.1371/journal.pone.0057599, https://dx.plos.org/10.1371/journal.pone.0057599, 2013.

Liu, Y. Y., Van Dijk, A. I., De Jeu, R. A., Canadell, J. G., McCabe, M. F., Evans, J. P., and Wang, G.: Recent reversal in loss of global terrestrial biomass, Nature Climate Change, 5, 470–474, https://doi.org/10.1038/nclimate2581, 2015.

Meesters, A., DeJeu, R., and Owe, M.: Analytical Derivation of the Vegetation Optical Depth From the Microwave Polarization Difference Index, IEEE Geoscience and Remote Sensing Letters, 2, 121–123, https://doi.org/10.1109/LGRS.2005.843983, http://ieeexplore.ieee.org/document/1420287/, 2005.

Meier, W., JesefinoC, C., and Thorsten, M.: NRT AMSR2 Unified L3 Daily 25 km Brightness Temperature & Sea Ice Concentration Polar Grids V1, https://doi.org/undefined, http://undefined, 2018.

Mikalsen, K. Ø., Bianchi, F. M., Soguero-Ruiz, C., and Jenssen, R.: Time series cluster kernel for learning similarities between multivariate time series with missing data, Pattern Recognition, 76, 569–581, https://doi.org/10.1016/J.PATCOG.2017.11.030, https://www.sciencedirect.com/science/article/pii/S0031320317304843, 2018.

Mo, T., Choudhury, B. J., Schmugge, T. J., Wang, J. R., and Jackson, T. J.: A model for microwave emission from vegetation-covered fields, Journal of Geophysical Research, 87, 11 229, https://doi.org/10.1029/JC087iC13p11229, http://doi.wiley.com/10.1029/JC087iC13p11229, 1982.

Moesinger, L., Dorigo, W., De Jeu, R., Van der Schalie, R., Scanlon, T., Teubner, I., and Forkel, M.: The Global Long-term Microwave Vegetation Optical Depth Climate Archive VODCA [Data set], https://doi.org/10.5281/ZENODO.2575599, https://zenodo.org/record/2575599{#}.XIjXc4Uo82A, 2019.

Momen, M., Wood, J. D., Novick, K. A., Pangle, R., Pockman, W. T., McDowell, N. G., and Konings, A. G.: Interacting Effects of Leaf Water Potential and Biomass on Vegetation Optical Depth, Journal of Geophysical Research: Biogeosciences, 122, 3031–3046, https://doi.org/10.1002/2017JG004145, http://doi.wiley.com/10.1002/2017JG004145, 2017.

Morton, D. C., Nagol, J., Carabajal, C. C., Rosette, J., Palace, M., Cook, B. D., Vermote, E. F., Harding, D. J., and North, P. R. J.: Amazon forests maintain consistent canopy structure and greenness during the dry season, Nature, 506, 221–224, https://doi.org/10.1038/nature13006, http://www.nature.com/articles/nature13006, 2014.

Myneni, R., Knyazikhin, Y., and Park, T.: MCD15A2H MODIS/Terra+Aqua Leaf Area Index/FPAR 8-day L4 Global 500m SIN Grid V006 [Data set], https://doi.org/doi: 10.5067/MODIS/MCD15A2H.006, 2015.

Myneni, R. B., Yang, W., Nemani, R. R., Huete, A. R., Dickinson, R. E., Knyazikhin, Y., Didan, K., Fu, R., Negrón Juárez, R. I., Saatchi, S. S., Hashimoto, H., Ichii, K., Shabanov, N. V., Tan, B., Ratana, P., Privette, J. L., Morisette, J. T., Vermote, E. F., Roy, D. P., Wolfe, R. E., Friedl, M. A., Running, S. W., Votava, P., El-Saleous, N., Devadiga, S., Su, Y., and Salomonson, V. V.: Large seasonal swings in leaf area of Amazon rainforests., Proceedings of the National Academy of Sciences of the United States of America, 104, 4820–3, https://doi.org/10.1073/pnas.0611338104, http://www.ncbi.nlm.nih.gov/pubmed/17360360http://www.pubmedcentral.nih.gov/articlerender.fcgi?artid=PMC1820882, 2007.

Njoku, E., Ashcroft, P., Chan, T., and Li Li: Global survey and statistics of radio-frequency interference in AMSR-E land observations, IEEE Transactions on Geoscience and Remote Sensing, 43, 938–947, https://doi.org/10.1109/TGRS.2004.837507, http://ieeexplore.ieee.org/document/1424270/, 2005.

Owe, M., de Jeu, R., and Holmes, T.: Multisensor historical climatology of satellite-derived global land surface moisture, Journal of Geophysical Research, 113, F01 002, https://doi.org/10.1029/2007JF000769, http://doi.wiley.com/10.1029/2007JF000769, 2008.

Saleska, S. R., Didan, K., Huete, A. R., and da Rocha, H. R.: Amazon forests green-up during 2005 drought., Science (New York, N.Y.), 318, 612, https://doi.org/10.1126/science.1146663, http://www.ncbi.nlm.nih.gov/pubmed/17885095, 2007.

Samanta, A., Ganguly, S., Hashimoto, H., Devadiga, S., Vermote, E., Knyazikhin, Y., Nemani, R. R., and Myneni, R. B.: Amazon forests did not green-up during the 2005 drought, Geophysical Research Letters, 37, n/a–n/a, https://doi.org/10.1029/2009GL042154, http://doi.wiley.com/10.1029/2009GL042154, 2010.

Samanta, A., Ganguly, S., Vermote, E., Nemani, R. R., Myneni, R. B., Samanta, A., Ganguly, S., Vermote, E., Nemani, R. R., and Myneni, R. B.: Why Is Remote Sensing of Amazon Forest Greenness So Challenging?, Earth Interactions, 16, 1–14, https://doi.org/10.1175/2012EI440.1, http://journals.ametsoc.org/doi/abs/10.1175/2012EI440.1, 2012.

Sawada, Y., Tsutsui, H., Koike, T., Rasmy, M., Seto, R., and Fujii, H.: A field verification of an algorithm for retrieving vegetation water content from passive microwave observations, IEEE Transactions on Geoscience and Remote Sensing, 54, 2082–2095, https://doi.org/10.1109/TGRS.2015.2495365, http://ieeexplore.ieee.org/document/7331296/, 2016.

Simard, M., Pinto, N., Fisher, J. B., and Baccini, A.: Mapping forest canopy height globally with spaceborne lidar, Journal of Geophysical Research, 116, G04 021, https://doi.org/10.1029/2011JG001708, http://doi.wiley.com/10.1029/2011JG001708, 2011.

Song, X.-P., Hansen, M. C., Stehman, S. V., Potapov, P. V., Tyukavina, A., Vermote, E. F., and Townshend, J. R.: Global land change from 1982 to 2016, Nature, 560, 639–643, https://doi.org/10.1038/s41586-018-0411-9, http://www.nature.com/articles/s41586-018-0411-9, 2018.

Teubner, I. E., Forkel, M., Jung, M., Liu, Y. Y., Miralles, D. G., Parinussa, R., van der Schalie, R., Vreugdenhil, M., Schwalm, C. R., Tramontana, G., Camps-Valls, G., and Dorigo, W. A.: Assessing the relationship between microwave vegetation optical depth and gross primary production, International Journal of Applied Earth Observation and Geoinformation, 65, 79–91, https://doi.org/10.1016/j.jag.2017.10.006, http://dx.doi.org/10.1016/j.jag.2017.10.006, 2018.

Teubner, I. E., Forkel, M., Camps-Valls, G., Jung, M., Miralles, D. G., Tramontana, G., van der Schalie, R., Vreugdenhil, M., MÃ¶singer, L., and Dorigo, W. A.: A carbon sink-driven approach to estimate gross primary production from microwave satellite observations, Remote Sensing of Environment, 229, 100 – 113, https://doi.org/https://doi.org/10.1016/j.rse.2019.04.022, http://www.sciencedirect.com/science/article/pii/S0034425719301671, 2019.

Tian, F., Wigneron, J.-P., Ciais, P., Chave, J., Ogée, J., Peñuelas, J., Ræbild, A., Domec, J.-C., Tong, X., Brandt, M., Mialon, A., Rodriguez-Fernandez, N., Tagesson, T., Al-Yaari, A., Kerr, Y., Chen, C., Myneni, R. B., Zhang, W., Ardö, J., and Fensholt, R.: Cou-

pling of ecosystem-scale plant water storage and leaf phenology observed by satellite, Nature Ecology & Evolution, 2, 1428–1435, https://doi.org/10.1038/s41559-018-0630-3, http://www.nature.com/articles/s41559-018-0630-3, 2018.

van der Schalie, R., de Jeu, R., Kerr, Y., Wigneron, J., Rodríguez-Fernández, N., Al-Yaari, A., Parinussa, R., Mecklenburg, S., and Drusch, M.: The merging of radiative transfer based surface soil moisture data from SMOS and AMSR-E, Remote Sensing of Environment, 189, 180–193, https://doi.org/10.1016/J.RSE.2016.11.026, https://www.sciencedirect.com/science/article/pii/S0034425716304734, 2017.

van Marle, M. J. E., van der Werf, G. R., de Jeu, R. A. M., and Liu, Y. Y.: Annual South American forest loss estimates based on passive microwave remote sensing (1990–2010), Biogeosciences, 13, 609–624, https://doi.org/10.5194/bg-13-609-2016, https://www.biogeosciences.net/13/609/2016/, 2016.

Vreugdenhil, M., Dorigo, W. A., Wagner, W., de Jeu, R. A. M., Hahn, S., and van Marle, M. J. E.: Analyzing the Vegetation Parameterization in the TU-Wien ASCAT Soil Moisture Retrieval, IEEE Transactions on Geoscience and Remote Sensing, 54, 3513–3531, https://doi.org/10.1109/TGRS.2016.2519842, 2016.

Vreugdenhil, M., Hahn, S., Melzer, T., BauerMarschallinger, B., Reimer, C., Dorigo, W. A., and Wagner, W.: Assessing Vegetation Dynamics Over Mainland Australia With Metop ASCAT, IEEE Journal of Selected Topics in Applied Earth Observations and Remote Sensing, 10, 2240–2248, https://doi.org/10.1109/JSTARS.2016.2618838, http://ieeexplore.ieee.org/document/7762756/, 2017.

Wentz, F. J.: A well-calibrated ocean algorithm for special sensor microwave / imager, Journal of Geophysical Research: Oceans, 102, 8703–8718, https://doi.org/10.1029/96JC01751, http://doi.wiley.com/10.1029/96JC01751, 1997.